Changes in the North Atlantic Climate System 2005-2016

Jon Robson[1,*], Alex Archibald[2], Fenwick Cooper[3], Matthew Christensen[4,3], Lesley J. Gray[3], N. Penny Holliday[5], Claire Macintosh[6], Malcolm McMillan[7], Ben Moat[5], Maria Russo[2], Rowan T. Sutton[1], Rachel Tilling[7], Ken Carslaw[8], Damien Desbruyères[5,9], Owen Embury[6], Daniel L. Feltham[10], Daniel P. Grosvenor[8], Simon Josey[5], Brian King[5], Alastair Lewis[11], Gerard D. McCarthy[5,12], Chris Merchant[6], Adrian L. New[5], Christopher H. O'Reilly[3], Scott M. Osprey[3], Katie Read[11], Adam Scaife[13,14], Andrew Shepherd[7], Bablu Sinha[5], David Smeed[5], Doug Smith[13], Andrew Ridout[15], Tim Woollings[3] , Ming Xi Yang[16]

Affiliations:

1. National Centre for Atmospheric Science, Department of Meteorology, University of Reading, Reading, UK

2. National Centre for Atmospheric Science, Department of Chemistry, University of Cambridge, Cambridge, UK

3. Atmosphere, Ocean and Planetary Physics, University of Oxford, Oxford, UK

4. STFC Rutherford Appleton Laboratory, Oxford, UK

5. National Oceanography Centre, Southampton, UK

6. National Centre for Earth Observation, Department of Meteorology, University of Reading, Reading, UK

7. Centre for Polar Observations and Modelling, University of Leeds, Leeds, UK

8. National Centre for Atmospheric Science, School of Earth and Environment, University of Leeds, Leeds, UK

9. IFREMER, Laboratoire d'Océanographie Physique et Spatiale, Plouzané, France

10. Centre for Polar Observations and Modelling, Department of Meteorology, University of Reading, Reading, UK

11. National Centre for Atmospheric Science, University of York, York, UK

12. Irish Climate Analysis and Research UnitS (ICARUS), Department of Geography, National University of Ireland Maynooth, Ireland

13. Met Office Hadley Centre, Exeter, UK

14. College of Engineering, Maths and Physical Science, University of Exeter, Exeter, UK

15. Centre for Polar Observations and Modelling, University College London, London, UK

16. Plymouth Marine Laboratory, Plymouth, UK

Abstract

Major changes are occurring across the North Atlantic climate system, including in the atmosphere, ocean and cryosphere, and many observed changes are unprecedented in instrumental records. As the changes in the North Atlantic directly affect the climate and air quality of the surrounding continents, it is important to fully understand how and why the changes are taking place, not least to predict how the region will change in the future. To this end, this paper characterises the recent changes in the North Atlantic region, especially in the period 2005—2016, across many different aspects of the system including: atmospheric circulation; atmospheric composition; clouds and aerosols; ocean circulation and properties; and the cryosphere. Recent changes include: an increase in the speed of the North Atlantic jet stream in winter; increases in ozone and methane; increases in net absorbed radiation in the mid-latitude western Atlantic, linked to an increase in the abundance of high level clouds and a reduction in low level clouds; cooling of sea surface temperatures (SST) in the North Atlantic subpolar gyre, concomitant with increases in the western subtropical gyre, and a decline in the Atlantic Ocean's overturning circulation; a decline in Atlantic sector Arctic sea-ice and rapid melting of the Greenland Ice Sheet. There are many interactions between these changes, but these interactions are poorly understood. The paper concludes by highlighting some of the key outstanding questions.

1. Introduction

The North Atlantic has warmed considerably over the past 100 or so years (Stocker et al., 2013). However, the North Atlantic has also evolved somewhat differently to the rest of the world's oceans on multi-decadal time scales, with periods of faster warming and cooling. This variability, which has become known as Atlantic Multi-decadal Variability (AMV, Sutton et al., 2017), has been linked to a wide range of impacts including rainfall anomalies over Africa, North America and Europe (Knight et al., 2006; Sutton and Dong, 2012; Sutton and Hodson, 2005); the frequency of Hurricanes (Smith et al., 2010; Zhang and Delworth, 2006); the rate of Greenland Ice-sheet melt (Holland et al., 2008); sea-level anomalies (Gerard D. McCarthy et al., 2015); fisheries (Hátún et al., 2009) and the strength of the mid-latitude atmospheric jet (Woollings et al., 2015). Therefore, uncertainty in how North Atlantic surface temperatures might change is a major uncertainty in climate projections, especially for the European sector (Woollings et al., 2012).

Although multi-decadal variability has been observed in the North Atlantic the mechanisms and processes that control this variability are poorly understood. A leading hypothesis is that changes in the strength of the ocean circulation, and particularly the Atlantic Meridional Overturning Circulation (AMOC), is an important contributor to the variability in the ocean heat content and sea surface temperature (Ba et al., 2014; Knight, 2005; Menary et al., 2015). However, a paucity of observations has prevented a direct link being made between ocean circulation changes and AMV in the real world, and there is a considerable diversity in the mechanisms of variability found in climate models (Ba et al., 2014; Menary et al., 2015). Variability in the atmospheric circulation is also an important driver of climate variability across the North Atlantic Climate system. The leading mode of atmospheric variability, the North Atlantic Oscillation, drives inter-annual to

multi-decadal time-scale variability in variables that span the entire Atlantic Climate system, including SST, ocean circulation, Ozone, surface run off from Greenland and extreme temperatures and rainfall over Europe (Hanna et al., 2014; Hurrell et al., 2003; Pausata et al., 2012; Robson et al., 2012; Scaife et al., 2008). Indeed, the NAO is often considered a major driver of AMOC, and hence AMV (Eden and Willebrand, 2001; Robson et al., 2012; Sutton et al., 2017). The NAO may also be influenced by AMV or other changes in North Atlantic conditions (Gastineau et al., 2013; Gastineau and Frankignoul, 2014; O'Reilly et al., 2017; Peings and Magnusdottir, 2014). However, unravelling the two way interactions between ocean and atmosphere is very challenging, especially in the short observational record.

A further question to consider is the role of external factors in driving changes in the North Atlantic. For example, recent studies have suggested that AMV is a result of competition between rising greenhouse gas emissions and regional changes in sulphate aerosols (Booth et al., 2012). Changes in solar irradiance and volcanic aerosols are also thought to be important influences on the atmospheric circulation and the NAO, and hence could impact widely across the North Atlantic climate system (Gray et al., 2013; Menary et al., 2013; Ortega et al., 2015). The long-term warming trend due to greenhouse gases is also changing the climate of the North Atlantic region, especially in the high-latitudes, including the Arctic and the Greenland Ice sheet (Stocker et al., 2013). Finally, the presence of global teleconnections, in the atmosphere in particular, means that variability and changes outside the North Atlantic can also have a substantial influence (Bell et al., 2009; Biastoch et al., 2008).

97 The composition of the atmosphere in the North Atlantic region has also been changing, and can
98 interact with changes in physical aspects of the climate. Ozone (O_3) and methane (CH_4) are
99 powerful greenhouse gases and can affect climate by changing the Earth's radiative balance
100 (Stocker et al., 2013). Tropospheric ozone can also affect human health and agricultural yields
101 (Kampa and Castanas, 2008), and was recently suggested to cause 1.2 million premature deaths
102 per year ((Malley et al., 2017)). Observed ozone changes are driven by a complex interplay of
103 emission changes in nitrogen oxides and organic and inorganic radicals changes in downward
104 transport from the stratosphere, and changes in regional circulation affecting transport timescales
105 (see e.g. Monks et al. (2015) for more details). However, while recent trends in Carbon monoxide
106 and methane are generally driven by emission changes (Nisbet et al., 2016; Worden et al., 2013),
107 the recent observed trends in ozone over the North Atlantic are not fully characterised or
108 understood (Parrish et al., 2014).
109
110 It follows from the above discussion that there are many important unanswered questions
111 regarding the nature of decadal time-scale change in the North Atlantic region. This lack of
112 understanding is a fundamental limit to our ability to understand the current changes, and also to
113 our ability to make quantitative predictions of how the North Atlantic climate system will change
114 in the future. However, the large number of processes involved, and complex array of interactions
115 between different components of the North Atlantic climate system, makes understanding the
116 ongoing changes in the North Atlantic challenging. Therefore, in order to improve our
117 understanding, this paper aims to characterise and document changes across multiple
118 components of the North Atlantic climate system. It focuses on the recent period (since 2000),
119 exploiting the many new observations that have recently become available as a consequence of

programmes such as ARGO and RAPID, and satellite products. The period 2006-2015/16 is a particular focus.

This paper is structured as follows. Recent changes in Atmospheric circulation are described in section 2, before recent changes in atmospheric composition are discussed in section 3. Recent changes in aerosols, clouds and radiative effects are described in 4, before changes in ocean properties and the cryosphere are discussed in sections 5 and 6. Finally, a summary and conclusions is presented in section 7.

2. Recent changes in atmospheric circulation and properties

In this section, we consider the recent variability and trends in atmospheric circulation over the North Atlantic region. We use data from the ERA-interim reanalysis (Dee et al., 2011) and where stated, the AIRS satellite (e.g. (Tian and National Center for Atmospheric Research Staff (eds), 2016)).

"The North Atlantic Oscillation (NAO) is one of the most prominent and recurrent patterns of atmospheric circulation variability" (Hurrell et al., 2003). It can be defined as the first empirical orthogonal function (EOF) of surface pressure in the region 30°W-40°E and 20°-70°N and its time evolution can be illustrated by plotting the corresponding principal component time-series. An alternative that does not require knowledge of surface pressure over this extended region, and can be derived easily from station-based observations, is the monthly mean Reykjavík-Gibraltar normalised difference in surface pressure (NAO_{R-G}, (Jones et al., 1997)). The two indicators are very

142 similar in the winter season (December-January-February; DJF), with a correlation coefficient of
143 0.89 over the period 1979-2016.
144
145 The recent NAO_{R-G} index averaged over the winter months (DJF) is plotted in Figure 1a. The
146 smoothed 11-year running mean of NAO_{R-G} increases from the mid-1980s, peaks around the early
147 1990s, and is followed by a downward trend (Woollings et al., 2015). The winter of DJF 2009/10
148 exhibits a particularly strong negative NAO, although positive values in the more recent years may
149 indicate a positive trend. To focus more on how the atmospheric circulation has varied over the
150 North Atlantic Ocean we also derive the EOF based index of the NAO (NAO_{Atl}) using the 1st EOF of
151 surface pressure over the restricted region 60-0°W and 30-70°N (Fig. 1b; see also Fig. S1a). In
152 comparison with NAO_{R-G}, the 11-year running mean of NAO_{Atl} in DJF is noticeably flatter with
153 respect to its variance, although the correlation of the DJF NAO_{Atl} with NAO_{R-G} is still 0.82. The 11-
154 year running mean of NAO_{Atl} for the summer months (June-July-August; JJA; Fig. 1c, with
155 corresponding EOF in Fig S1c) has been on a continuous downward trend since 1990. (We note
156 from examination of the structure of the first EOF of the JJA surface pressure that the station-
157 based NAO_{R-G} is not an appropriate indicator of the summer-time circulation (compare A2a and
158 A2b.) and it is therefore not shown).
159
160 While the NAO is a useful single indicator of atmospheric circulation over the Atlantic and its
161 potential impact on European weather, it is nevertheless a derived quantity combining several
162 factors. Two additional indicators that directly characterise the North Atlantic Jetstream have been
163 proposed: the jet latitude and jet speed (Woollings et al., 2014). Figures 2a,b show the DJF and JJA
164 time-series of zonal velocity at 850 hPa in the region 60-0°W and 15-75°N, to illustrate the spatial

evolution of the mid-latitude Jetstream. The jet latitude index (JLI) is defined as the latitude of the maximum zonal wind speed at 850 hPa calculated using seasonal mean zonal winds over the region 60-0°W, 15-75°N (Figs. 2c,d). The JLI is clearly related to NAO_{Atl} (compare figures 1b / 2c, and 1c / 2d); positive NAO_{Atl} implies that the jet maximum is somewhat offset to the north. Figure 2c shows that recent trends in the 11-year running mean of the winter JLI are small in comparison with the interannual variability (Woollings et al., 2014). The recent trend in 11-year running mean of the summer JLI (Fig. 2d) is southwards, consistent with the negative trend in NAO_{Atl}. Note the different scales in Figures 2c,d indicating that variability in winter JLI is larger than in summer.

The jet speed index (JSI; Figs 2e,f) is defined as the maximum zonal velocity in the region 60-0°W at the latitude identified by the JLI. It is also more variable in winter than in summer. The 11-year running mean of the winter jet speed peaks in 1990, is a minimum around 2005, and then returns to higher speeds more recently. As the summertime jet has moved southwards in recent years it has also weakened (Fig. 2f). Figure 2f also hints that variability in the JJA mean jet speed has reduced.

Comparing the NAO and jet indices we can see that the negative summer NAO trend over 2005—2016 (Fig 1c) largely reflected an equatorward jet shift (Fig2d), with some contribution of a weaker jet (Fig 2f). In the winter, the trend over 2005—2016 was to a slightly stronger jet (Fig 2e). However, the interannual variability in jet latitude (Fig 2c) also made an important contribution to the interannual evolution of the NAO (Fig 1a). Nevertheless, these changes in the zonal wind speed and latitude have implications for atmospheric heat and water vapour (Deser et al., 2010) and aerosol (Lewis and Schwartz, 2004) exchange with the Atlantic Ocean, as has been pointed out

for the Southern Ocean (Korhonen et al., 2010). The equatorward migration of the summertime jet may be linked to Atlantic Multidecadal Variability (Sutton and Dong, 2012), which transitioned from negative to positive in the mid-1990s (Sutton et al., 2017).

Figure 3 shows trends in the overall seasonal surface pressure fields (rather than only the NAO index). In DJF for both the 1990-2005 and 2006-2016 periods, the pressure trends project strongly onto the second EOF pattern. The dot products of these trends with the second EOF patterns (not shown), both normalised to unit vectors, are 81% and 76% respectively, while their projection onto the first EOF pattern is weaker (19% and 51% respectively). In JJA on the other hand the situation is reversed with stronger projection of trends onto the first EOF (55% and 56% respectively) than onto the second EOF (17% and 12% respectively).

In Figure 3 the hatched regions indicate where there is less than a 5% chance (i.e. $p \leq 0.05$) that the observed trend is consistent with random variability. We conclude that trends in the seasonal mean surface pressure over the periods considered are small relative to its variance, and the trends will be sensitive to the time periods used. However, over the period 1990-2005 there was a statistically significant increase in pressure over Greenland. This increase suggests that the 11-year decreasing trend in NAO over this period (Figs 1a,b) is primarily associated with a weakening of the Icelandic Low (i.e. the northern node of the NAO). Despite a stronger (positive) trend over 2006-2016 when compared to 1989-2005, the 2006-2016 trend is not significantly different from that expected from random numbers (note also the slightly shorter time period). The summertime pressure trends are smaller than the wintertime trends, but note that this could be due to the smaller variability in summertime.

As an illustration of the vertical distribution of recent circulation changes, Figure 4 shows the zonally-averaged DJF zonal wind at 60°N. Year to year changes in the strength of the extratropical westerly jet stream tend to be equivalent barotropic and hence vertically aligned throughout the depth of the troposphere and stratosphere. There is also sometimes additional evidence for a downward propagation of zonal wind changes and they show some striking inter-decadal variability. Recent decades have shown substantial variability in the strength of these extratropical winter westerlies. A build-up of strong westerlies occurred from the early 1960s (see e.g. Figure 3 in (Scaife et al., 2005)), and is apparent throughout the depth of the atmosphere, eventually peaking in the early 1990s, as evident in Figure 4. These early 1990s winters also coincided with a string of positive episodes of the surface North Atlantic Oscillation and were accompanied by intense storms, very wet winters and a drastic reduction in the number of frost days in northern Europe (Roberts et al., 2014; Scaife et al., 2008). While the build-up of the westerlies in the early 1990s seen in figure 4 is related to multi-decadal variability rather than a systematic trend, the reasons are still unclear. It is not even known if this is due to forced or internal variability. Proposed explanations involve internal chaotic variability (Semenov et al., 2008), ocean-atmosphere interaction (Hoerling et al., 2004; Omrani et al., 2016) and forced responses to volcanism (Driscoll et al., 2012; Marshall and Scaife, 2009) or solar variability (Gray et al., 2010; Ineson et al., 2011).

Following the peak in the 1990s, a subsequent decline in the winter westerlies is evident in Figure 4, with a deep minimum in 2010 that corresponds to the strongly negative NAO in Figures 1a,b. Although the maximum easterly anomalies are in the troposphere, there is evidence of downward

234 extension from the stratosphere. The 2010 anomaly is also visible as an equator-ward shift in the
235 position of the Atlantic westerlies (Fig.2a). The winter of 2009/10 exhibited the lowest NAO on
236 record (Cattiaux et al., 2010; Fereday et al., 2012; Seager et al., 2010) and the coldest December
237 for a century (Blaker et al., 2015; Maidens et al., 2013). The cause of the 2009/10 weak westerlies
238 is at least partly understood in terms of the extratropical response to El Nino (Fereday et al.,
239 2012), the deep minimum in the 11-year solar cycle (Gray et al., 2013, 2016) and the easterly
240 phase of the QBO (Fereday et al., 2012; Pascoe et al., 2006).
241
242 After 2010 the westerlies strengthened again. The recent three winters from 2013/14 to 2015/16
243 were all strong westerly winters with positive surface NAO and numerous winter wind storms and
244 abundant rainfall (Huntingford et al., 2014; Scaife et al., 2017; Watson et al., 2016; Wild et al.,
245 2015). Recent changes in the Atlantic Ocean surface conditions and tropical rainfall help to explain
246 this recent upturn, which also closely follows the recent solar maximum (Scaife et al., 2017).
247
248 North Atlantic sea surface temperatures are strongly influenced by atmospheric seasonal
249 variability (see section 5 of this paper and, for example, Deser et al. 2010). However, surface heat
250 fluxes are governed by a complex function of the wind speed, humidity and temperature
251 differences (e.g. Hewitt et al., 2011, their Fig. 1). The 2006-2016 trend in ERA-interim 2m
252 temperature is plotted in Fig. 5a (DJF) and 5b (JJA). The DJF cooling in the North Atlantic region is
253 visible above the background variability, consistent with the 1996-2005 sea surface temperature
254 trends in figure 14. The summertime trend (JJA) over this time period is smaller, but shows the
255 same overall pattern of a cooling in the north Atlantic, including over Greenland, and a warming
256 further towards the tropics.

To examine trends at higher levels the 2006-2016 trends in the seasonal mean 700 hPa air temperature are plotted in figures Fig. 5c and 5d (now as measured by AIRS, to be consistent with the water mass mixing ratio plots in Fig 5e and 5f). Although barely distinguishable from the background variability, both the wintertime and summer time 700 hPa trends bear some resemblance to their 2m equivalents. In DJF, the north Atlantic has cooled at 700hPa by around 0.15^{o}C per decade, while warming towards the tropics and the wintertime trend is again much larger than the summertime. Trends in the 700 hPa water mass mixing ratio (as measured by AIRS) are not distinguishable from the background variability over this time period. It is not clear how closely the trend patterns for water mass mixing ratio in both DJF and JJA (of around 0.0025 g/kg dry air) reflect the respective 700 hPa temperature trend patterns in the north Atlantic.

3. Recent changes in atmospheric composition

In this section we concentrate on tropospheric ozone and methane; two important trace gases for which a recent satellite record exists. Ozone is produced in the troposphere through a complex interplay of reactions involving nitrogen oxides and organic and inorganic radicals (see e.g. Monks et al. (2015) for more details). Because of its short lifetime in the troposphere (days to weeks), the largest ozone concentrations are often observed downwind but in close proximity to the sources of precursor gases. Methane on the other hand, has a much longer lifetime in the troposphere (around 10 years) and is relatively well mixed. Changes in methane concentrations are generally thought to be mainly driven by changes in its emissions, which range from soils in natural wetlands through to fossil fuel production. More recently changes in methane concentrations have also been attributed to changes in the concentration of the hydroxyl radical (OH), the main sink for

methane, (Prather and Holmes, 2017; Rigby et al., 2017; Schaefer et al., 2016; Turner et al., 2017). In this section we document recent changes using surface observations and monthly-mean gridded satellite data from OMI/MLS and AIRS to investigate trends in tropospheric ozone (Ziemke et al., 2006) and methane (Xiong et al., 2008; Yurganov et al., 2008) respectively.

3.1 Timeseries of surface ozone at selected monitoring sites, tropospheric ozone column and total methane column

Figure 6 shows recent trends (ca 2006 - 2016) of ozone and methane in the North Atlantic as measured at the surface and by satellite. Surface ozone shows a strong seasonal cycle across the North Atlantic, with a peak in spring and a minimum in the summer (see figure 6 b). Surface ozone at Bermuda has been decreasing significantly at a rate of 19.8 ppb/decade; this is likely due to the significant reduction in emissions of ozone precursors in the USA (Granier et al., 2011). A smaller decrease is observed at Mace Head; in this case, the changes are harder to attribute and may reflect local changes to the lifetime of ozone or the effect of large decreases in ozone precursors upwind of Mace Head. In contrast, surface ozone at Cape Verde has been increasing at a rate of 3.6 ppb/decade. This may be related to an increase in shipping, and hence ozone precursor emissions, a decrease in oceanic halogens, an important sink for ozone (Read et al., 2008), or a general effect of the increases in methane, which acts as an important ozone precursor at the global scale (Young et al., 2013).

Changes in tropospheric ozone column, fig 6c, show a different picture, with a consistent increase across the North Atlantic. Several factors can contribute to trends in background tropospheric ozone including changes in emissions of ozone precursors, changes in temperature and solar

radiation and long range transport of ozone and its precursors. It has also been suggested that through El Niño/Southern Oscillation and the stratospheric Quasi-Biennial Oscillation, large scale changes in climate may be affecting the transport of stratospheric rich ozone into the troposphere (Neu et al., 2014) thereby increasing the tropospheric ozone burden.

The satellite retrievals of total column methane also show a strong, near linear, increase in methane over the North Atlantic in the last decade. This is consistent with our current understanding of global methane trends, e.g. (Nisbet et al., 2016). The methane trends are consistent across sub-regions of the North Atlantic, albeit the total column methane magnitude is smaller in the subtropics than in the mid-latitudes. A lower subtropical methane column is consistent with a shorter lifetime (due to higher concentrations of OH), weaker primary sources and stronger mixing into the stratosphere (through deep convection) in the tropics compared to mid latitudes.

3.2 Spatial and seasonal variability in observed trends

In this section, we analyse how trends in the observed columns of ozone and methane vary spatially and seasonally across the North Atlantic basin. Methane is a relatively long lived gas which is generally well mixed at a regional scale and therefore very little spatial and seasonal variation in the North Atlantic trends is observed (not shown). On the other hand, ozone shows some interesting spatial variations with generally positive trends ranging between 0 and 15% per decade, depending on location. In winter (top panels of figure 7) the spatial variability of ozone trends becomes larger with negative ozone trends over the Western part of the North Atlantic domain and very large positive trends over Central Europe and the Eastern part of the North

Atlantic basin. In summer (middle panels in figure 7) ozone shows a larger increase in the subtropical North Atlantic.

Observations from a small number of surface stations in the nineteenth century indicate that ozone concentrations have increased significantly since preindustrial times due to anthropogenic activities (Mickley et al., 2001; Shindell et al., 2006; Stevenson et al., 2013). In developed countries, a recent reduction in the emissions of ozone precursors (Granier et al., 2011) has helped decrease ozone levels and made an impact at the local and regional scale. However, different observational studies do not provide a consistent picture regarding the sign and magnitude of recent ozone trends at northern mid-latitudes (Cooper et al. 2014, Parrish et al. 2014, Ebojie et al. 2016, Oetjen et al. 2016). Our study shows a generally small, but significant, positive trend over the North Atlantic for the period 2006-2016 (figure 6c and Fig 7). The ozone increase seems to be larger and more robust for the subtropical North Atlantic, and also for summer compared to winter. Despite looking at similar quantities, i.e. tropospheric ozone column, our results and those of Ebojie et al. (2016) and Oetjen et al. (2016) all somewhat differ from each other. This is partly due to significant differences between the observing techniques and the different retrieval schemes applied. Similarly, the differences we identify between observed trends for surface and free tropospheric ozone are likely due to a decoupling between surface ozone (driven by local emission and sinks) and mid-tropospheric ozone (driven by large scale transport and STE).

3.3 Impact of NAO on North Atlantic composition and possible effects on observed ozone trends

The positive phase of the NAO can increase the rate of transport of ozone and ozone precursors from North America to Europe. Ozone has a relatively short lifetime; therefore, faster transport

across the North Atlantic can increase its abundance downwind of source regions. Changes in precipitation patterns (Scaife et al., 2008) associated with the positive phase of the NAO (wetter than average Northern Europe and drier than average Southern Europe) can additionally affect ozone distribution by affecting the concentration of soluble ozone precursors. The NAO can also have an impact on modulating strat-trop exchange (Simmonds et al., 2013) which in turn can affect the regional ozone distribution in the North Atlantic.

Several studies have looked at intercontinental transport of tracers and pollutants and the role of the NAO in such transport pathways (Creilson et al., 2003; Li et al., 2002; Pausata et al., 2012). Li et al. (2002) analysed modelled hourly surface ozone at Mace Head, for the period 1993-1997, and found it includes a significant fraction of North American ozone, around 10% on average throughout the year, and rising up to ~30% during transatlantic transport events. Creilson et al. (2003) analysed tropospheric ozone column (from TOMS/SBUV instruments) for the period 1979-2000 and found that, in some regions of the North Atlantic, tropospheric ozone is correlated to the NAO index. Similarly, Pausata et al. (2012) found a correlation between the winter NAO index and ozone concentrations from stations in the UK and Northern Europe. They further suggested that summer NAO events could increase ozone concentrations over Europe, at a time when ozone levels are generally highest and could pose a threat to human health. As the NAO exerts a large influence on ozone transport over the North Atlantic, understanding future changes in the NAO and its influence on atmospheric composition is an important but little studied task (Bacer et al., 2016).

We now focus on whether we can identify any influence of the winter NAO on the tropospheric ozone data used for this study and address whether changes in the NAO could partly explain observed or future ozone trends in the North Atlantic. Figure 8 (top panel) shows the difference in monthly mean tropospheric ozone column between winter months with 'high' and 'low' NAO indices. The top panel of figure 8 suggests that the tropospheric ozone column decreases by up to 5-6 DU over large parts of North Europe, the UK and mid latitude North Atlantic when the NAO is in its positive phase compared to when it is in its negative phase. Conversely, large areas of North Africa and subtropical North Atlantic see an increase in tropospheric ozone column of 5-6 DU when the NAO is in its positive phase. This indicates a sizeable change in tropospheric ozone column over large areas of the North Atlantic (up to ~15%) when the NAO switches between different phases. Furthermore, the bottom panel in figure 8 shows that areas with the largest ozone changes are also strongly correlated to the winter NAO index. In conclusion, different phases of the NAO can alter ozone concentrations at a regional level. Therefore, a future trend in the winter NAO index could have a large impact on ozone trends across different regions of the North Atlantic.

4. Recent changes in aerosols, clouds and radiative fluxes

Recent changes in aerosol, cloud and top of atmosphere radiative fluxes are assessed across the North Atlantic Ocean using several mature satellite observation products. These satellite observations span multiple decades and cover a wide range of spatial (from 1 km) and temporal scales (in daily intervals over 30 years in selected satellite missions). Top-of-atmosphere (ToA) shortwave and longwave fluxes are obtained from the CERES-EBAF version 2.8 (Clouds and the Earth's Radiant Energy System Energy Balanced And Filled) product from the Terra satellite, and

393 the ESA-CCI (European Space Agency Climate Change Initiative) ATSR (Advanced Track Scanning
394 Radiometer) satellite derived fluxes using the ORAC (Optimal Retrieval for Aerosol and Cloud)
395 algorithm. ORAC-ATSR retrieves top of atmosphere radiative fluxes at the 1-km pixel-scale imager
396 resolution using BUGSrad, a correlated-k and Eddington approximation radiation model for
397 retrieving broadband fluxes (Stephens et al., 2001), in conjunction with the ORAC aerosol and
398 cloud retrieval (Christensen et al., 2016). Cloud and aerosol properties are analysed in MODIS
399 (MODerate Resolution Imaging Spectroradiometer) standard collection 6 data and ATSR ORAC
400 retrieval. Daytime data is averaged into monthly time intervals over 1°×1° regions. MODIS/CERES
401 provides data from the Terra satellite over the period from 2000 – present day. The ATSR satellite
402 series contain two satellites the ATSR-2 which provides observations from 1995 – 2003 and AATSR
403 provided data from 2002 – 2012.
404
405 **4.1 Observed trends**
406 The North Atlantic Ocean encompasses a variety of regional climates. Radiative fluxes across this
407 region are strongly influenced by the midlatitude storm track, dry subtropics where low-level
408 clouds interact with offshore Saharan dust, and deep convective clouds (Harrison et al., 1990).
409 Trends in the energy budget at the top of the atmosphere using 10 years (2006 – 2016) of CERES
410 observations are displayed in Figure 9. Net *radiative* cooling (south of the Azores; box 1 in figure
411 9c) and warming (in the West Atlantic, box 2 in figure 9c) trends are evident (we use the term
412 cooling to imply an increase in the net upward LW+SW radiation). The radiative changes in these
413 regions are correlated (mostly) to the changes in cloud cover fraction (influencing reflected
414 sunlight and hence shortwave radiative cooling, fig. 9d) and/or cloud-top pressure (influencing
415 longwave radiative emission, fig. 9e). Aerosols may also indirectly interact with these clouds

416 causing subsequent changes in their optical properties that typically cause shortwave radiative
417 cooling (Twomey, 1974), although this effect cannot be deduced from these data. Increases in
418 aerosol loading are apparent from the positive trend in aerosol optical depth (AOD) in a zonal strip
419 oriented off the African Saharan coast (fig. 9f). This increase is likely to be associated with dust
420 aerosol from the African continent, which may have implications for cloud ice nucleation (e.g.
421 Atkinson et al., 2013; Welti et al., 2017). The extent to which the increased aerosol loading off the
422 coast of Africa is affecting the cloud properties demands further investigation. On the other hand,
423 decreases in AOD occur off the east coast of the United States and Europe over the same period.
424
425 The East Atlantic box region (box 1) is related to an increase in the reflected shortwave radiative
426 flux, which is associated with the large increase in reflective low-level clouds (figure 10b and c),
427 and longwave radiative cooling, due to the negative cloud top pressure trends (i.e. cloud-top
428 height is increasing, Figure 9c). An evident seasonal cycle in cloud fraction is present in the East
429 Atlantic with the maximum cloud fraction occurring in winter in both the standard MODIS and
430 ATSR-ORAC retrieval (figure 10 b and c). In box 1, ATSR is found to retrieve a higher fraction of
431 low-level clouds than MODIS although ATSR tends to underestimate the total cloud fraction
432 relative to MODIS. This underestimation in ATSR is possibly due to weaker sensitivity using fewer
433 channels than MODIS (Poulsen et al., 2011).
434
435 In the West Atlantic (box 2) the positive net TOA flux trend corresponds to a negative trend in the
436 outgoing longwave radiation, which is associated with a decrease in cloud to pressure. This could
437 indicate an increase in cloud top heights, and/or an increase in high-level clouds that emit less
438 longwave radiation to space (i.e. trapping more heat in the troposphere). While smaller by

comparison, we also observe a reduction in low-level clouds during this period. Combined with the increase in overall cloud fraction in this region seen in Figure 9d, this indicates an increase in mid- and high-altitude cloud fraction. A decrease in low level cloud would give rise to radiative warming (when there is no overlying cloud). Therefore, both flux trends (shortwave and longwave) contribute to the substantial radiative warming trend in the West Atlantic region.

Trends were also examined for individual seasons (not shown). During DJF, the net radiative flux trends are similar and slightly amplified compared to the annual flux trends; this is particularly notable for the very strong positive aerosol optical depth trend off the coast of Saharan Africa. During JJA, the net radiative flux trends in the East Atlantic (i.e. box 1) reverse sign (i.e. they become positive) resulting in more energy absorption. This reversal in sign may be due to a decreasing cloud fraction trend during this season, possibly caused by decreasing aerosols.

4.2 Discussion

Here we have used mature satellite data products to examine the recent changes in aerosols, clouds and radiative fluxes across the North Atlantic Ocean and we have identified net radiative flux trends over the 2006—2016 period. Changes in cloud properties largely control the radiative flux responses. These changes may be caused by changes meteorological and/or atmospheric composition. For example, the regime switch from low-level to deeper-level clouds in the West Atlantic region (box 2) may be affected by changes in sea surface temperature, atmospheric stability, aerosols, or possibly numerous other related factors that need to be explored in subsequent work with high resolution models.

462 The North Atlantic Oscillation (NAO) also affects sea surface temperature and the thermodynamics
463 that influence cloud formation. The NAO may also drive strong cloud radiative feedbacks as
464 suggested by Yuan et al. 2016. For example, the positive phase of the NAO is associated with
465 weaker trade winds and reduced dust outflow and low-clouds off the coast of the Saharan desert,
466 which results in further warming of the tropical North SST's. This dynamical feedback, as described
467 in Yuan et al. 2016, is corroborated here by the correlation analysis with the NAO index (Figure
468 11a) and the top of atmosphere net cloud radiative effect (Figure 11b). The strong correlation
469 pattern (regions have Pearson correlation coefficients greater than 0.4) in the TOA radiative fluxes
470 and increase in dust outflow over this period implies there may indeed be a strong connection
471 between the NAO, cloud radiative effect, cloud fraction, and emission of dust aerosol (e.g. the
472 trends in Figure 9c are highly correlated to the correlation trend with the NAO in Figure 11b). By
473 including meteorological factors and comparing these trend results with regional-scale models the
474 process-scale interactions influencing cloud radiative feedbacks will advance our understanding of
475 the North Atlantic Climate system.
476

477 5. Recent Trends in Ocean Circulation and Properties

478 The Subpolar North Atlantic (SPNA) and Subtropical North Atlantic (STNA) are characterised by
479 large wind-driven gyres which meet at circa 45°N, where the upper ocean Gulf Stream/North
480 Atlantic Current system feeds subtropical water into the eastern SPNA. A warm net northward
481 flow is balanced by returning colder intermediate (1000-2000m) and deep layers (>2000m)
482 concentrated in the deep western boundary currents: the basic vertical structure of the Atlantic
483 Meridional Overturning Circulation (AMOC).
484

From 1996 to circa 2005 a range of indicators in the SPNA evolved in essentially the same way. For much of the record the upper ocean trend was to higher sea level, higher sea surface temperatures, and greater ocean heat content (see Figure 12). However the period since 2006 has shown a different pattern; that of surface cooling and decreasing heat content above 1000m (Fig. 14a-b). Some of the upper ocean and surface cooling can be explained by cold winters with high heat loss from the ocean to the atmosphere (Fig. 13f) (de Jong and de Steur, 2016; Duchez et al., 2016; Grist et al., 2016; Josey et al., 2015). Unusually deep convection (to 1600m) was observed in the Labrador Sea in winter 2014/15 (Yashayaev and Loder, 2016)], though the convection has not yet reached the depths observed during the last extended period of deep convection (1987-1994, 2100m) when the heat content was lower than it is today. The occurrence of cold winters, heat loss and convective activity is strongly associated with the sign of the NAO index. The cold conditions in the mid-1990s in Fig. 12 developed over 2 decades of increasingly positive NAO conditions (see fig. 1a-b), and the high heat loss in 2008, 2014 and 2015 were also under NAO positive conditions.

In the SPNA, heat loss to the atmosphere is replenished to a greater or lesser extent by the transport of heat in the upper ocean from the subtropics. This ocean heat transport is thought to be a dominant factor in setting multi-year patterns of SPNA upper ocean heat content (Robson et al., 2012; Williams et al., 2014). The mechanisms for ocean heat transport include the AMOC and the circulation of the gyres, and these may respond to different forcing on different timescales. A measure of decadal changes in heat transport from the STNA to the SPNA is given in an index derived from the sea level gradient along the eastern US coast (Gerard D. McCarthy et al., 2015), Fig. 13d). When a 7-year low-pass filter is applied, this index leads the rate of change of SPNA

surface temperature trends by around 2 years. The index is closely related to the NAO and matches the trend towards negative NAO from 2000 to 2011, reversing sharply in the previous few years in response to the shift to positive NAO. A measure of subpolar gyre heat transport is given by an index derived from sea surface height gradients across the region (Berx and Payne, 2016; Häkkinen and Rhines, 2004) (Fig. 13a). Multi-year periods of decreasing index imply a slowing gyre circulation in association with decreasing wind stress curl, increased occurrences of atmospheric blocking events (Hakkinen et al., 2011) which are linked to periods of warmer, more saline eastern SPNA. The decadal-scale trend in the index reflects the long-term change in basin-scale steric height (Foukal and Lozier, 2017).

SPNA sea level remains high despite the recent cooling (Fig 12a), even while the steric sea level contribution (from salinity and temperature) has decreased (Fig 12b). Some property changes are be density-compensating and do not directly contribute to sea level changes (Desbruyères et al., 2017; Mauritzen et al., 2012). For most of the 1993-2015 period the steric sea level component follows a very similar pattern to the upper ocean heat content, though Figure 14 shows that changes in salinity oppose the thermosteric changes to some extent. The mass component of total sea level rise (i.e. from ice loss, or changes in land water storage) is clearly significant in the SPNA.

At intermediate depths (1000-1800m) the SPNA is dominated by Labrador Sea Water (LSW). Formed in the Labrador and Irminger Seas by deep winter convection and freshened by mixing with Arctic-origin shallow outflows, the LSW spreads southward to form the upper part of the AMOC deep return flow. Since 1995, after the cessation of the last major deep convection period

in the Labrador Sea, this layer has been steadily warming and increasing in salinity as it re-stratifies and mixes with warm, saline boundary currents (Lazier et al., 2002), while elsewhere it also mixes with surrounding water types (Yashayaev et al., 2007). This means that since 2006 the SPNA intermediate layer has been changing in an opposite sense to the upper layer. The 2014/15 convection reached 1600m in the Labrador Sea (Yashayaev and Loder, 2016), but this localised event has apparently not yet impacted on the heat content averaged across the whole basin (Fig. 12i).

The data coverage in the deepest SPNA layer of dense northern overflows (>2000m) is restricted to locations where repeated measurements are made from ships and moored instruments. We observe in the overflows a small increase in salinity from 1996 to 2015 at the Iceland-Scotland ridge, a slight cooling at the Denmark Strait, and remarkably steady volume transport at both (see Fig. 13c) (Hansen et al., 2016; Jochumsen et al., 2012). By the time the overflows reach the Labrador Sea they have increased in volume by entraining upper layer and intermediate water, and thus we observe a much larger increase in salinity and density in the Labrador Sea between 1996 and 2015 (Yashayaev and Loder, 2016).

The LSW and overflows exit the subpolar gyre west of the Grand Banks, becoming known as the upper and lower North Atlantic Deep Water (NADW). NADW enters the subtropical gyre in the 'transition zone' (Buckley and Marshall, 2016) where it encounters the subtropical waters of the Gulf Stream extension. Some of the deep waters take interior pathways southwards (Bower et al., 2009; Lozier et al., 2013) but most form the deep western boundary current. By 30°N, the classical pattern of subtropical Atlantic circulation is established, with a horizontal gyre circulation in the

554 top 1000 m interacting with the large-scale overturning circulation (northwards in the top 1000m,
555 southward below 1000m) (Bryden and Imawaki, 2001). The balance of warm shallow waters
556 moving northwards, with cold deep waters coming southward, leads to the largest heat transport
557 of any ocean. Since 2004, the RAPID project has been measuring the AMOC at 26°N (G. D.
558 McCarthy et al., 2015).
559
560 Timescales of variability in the subtropical Atlantic differ from the subpolar North Atlantic. The
561 SPNA shows a more smooth, decadal scale variability and the STNA shows much more interannual
562 variability as it responds to local forcing as well as large-scale, longer term forcing (Bingham et al.,
563 2007). This is reflected in the time-series of heat content, SST and sea-level change in the last 20
564 years also (Fig. 12). While overall STNA sea level has risen in a similar manner to the SPNA
565 (reflecting perhaps the global trend in sea level rise), the steric sea level, SST and upper ocean heat
566 content anomaly show much more variable patterns in the STNA than the SPNA equivalents.
567 Interannual timescale variability in the subtropics complicates the comparison between the SPNA
568 and STNA but opposing patterns of variability are expected to be seen between the two gyres on
569 decadal to multidecadal timescales due to opposing wind driven circulation changes (Williams et
570 al., 2014).
571
572 The measurements from the RAPID array can be used to understand these processes. Large and
573 unexpected interannual variability was observed in the AMOC at 26°N in 2009 to 2010 (McCarthy
574 et al., 2012). The AMOC dropped in strength by 30% for a period of 18 months (Fig. 13b). This was
575 most likely wind-initiated (Roberts et al., 2013) and had the effect of cooling the subtropical ocean
576 through ocean heat transport divergence (Cunningham et al., 2013). However, a longer term

577 weakening of the AMOC has also been ongoing. The AMOC had a strength of 18.5 Sv from 2004-
578 2008 but only 15.5 Sv from 2009-2015 (updated from Smeed et al. 2014). Changes in the
579 transport of deep water masses had the largest influence on this 10-year decline. The decadal
580 slowdown in overturning is likely to warm the subtropics and cool the subpolar NA as it leads to a
581 reduction in heat exported from the subtopics to higher latitudes—a pattern that is consistent
582 with the evolution of heat content in both gyres since 2010.
583
584 The pattern of large-scale cooling associated with a reduction in strength of the overturning
585 circulation is linked, in climate models and reanalyses, to reduced densities in the deep Labrador
586 Sea (in those studies meaning 1000-2500m) (Jackson et al., 2016; Robson et al., 2014, 2016). In
587 observations this depth range is called the upper NADW (UNADW), which has its origins in the LSW
588 that is observed to have multi-decadal changes in density in the source region (Yashayaev and
589 Loder, 2016). However, direct signatures of Labrador Sea density changes such as those described
590 in (Ortega et al., 2011) have yet to be seen at 26°N. Disentangling these (predominantly wind-
591 driven) changes that cause the vertical displacement (or heave) of isopycnal surfaces from changes
592 driven by source water changes is a key problem in understanding the LSW-AMOC link.
593
594 In observations at 26°N the greatest changes in density and transport are in the lower NADW
595 (LNADW, 3000-5000m), which has origins in the dense overflows of the SPNA (Smeed et al., 2014).
596 To interpret the slowdown in LNADW transport in the STNA as a consequence of changes in the
597 overflows is an oversimplification. Indeed, as we have seen, the overflows have been remarkable
598 constant in their volume transport over the last 20 years. At 26°N and throughout the STNA, in
599 the depth range of NADW, density is higher on the western boundary than on the eastern

boundary, defining the velocity shear pattern allowing for southward flowing NADW. The density of the LNADW at 26°N has decreased on the western boundary since 2004, directly driving some of the weakening in the LNADW transports (Smeed et al. 2014, see their figure 6). The same pattern of deep density reduction is seen at 16°N (Frajka-Williams et al., 2016). At 26°N, a large amount of the total change in the LNADW transport reduction since 2004 appears as a compensation to thermocline/gyre changes in order to balance mass across the section. This mass constraint has been independently verified, within an accuracy of approximately 1 Sv, in models (Hirschi and Marotzke, 2007), by bottom pressure recorder data (Kanzow et al., 2007) and gravity satellite, GRACE, data (Landerer et al., 2015). While undoubtedly a real signal, the changes in LNADW due to compensation are perhaps less interesting that those due to the change in density. Deep density changes are the mechanism by which the AMOC collapses in a range of CMIP5 models under future greenhouse gas emissions scenarios (McCarthy et al., 2017) and perhaps offer the earliest hints of detectability of an AMOC collapse (Baehr et al., 2007).

A notable change in the STNA in the last 10 to 20 years has been a shift in the path of the Gulf Stream. This is most evident in patterns of sea level change (Fig. 14c to 14e) but also in trends in SST and upper ocean heat content (Fig. 14b and 14g). The Gulf Stream path is known to vary on multi-annual and longer timescales. This variability is characterized by meridional shifts in the position of the Gulf Stream extension known as the Gulf Stream North Wall (GSNW). The relationship between the GSNW and the AMOC is disputed with some authors arguing that a northward shift accompanies a strengthening AMOC (McCarthy et al., 2015) and other authors arguing that a southward shift accompanies a strengthening AMOC (Joyce and Zhang, 2010), with the latter view being supported by the patterns observed in the last decade.

6. Current state and recent changes in North Atlantic sea ice and the Greenland Ice Sheet

This section summarises the nature and drivers of recent changes to North Atlantic sea ice and the Greenland Ice Sheet. We first describe decadal variability in sea ice extent, regional ice concentration and sea ice volume. We then summarise the recent behaviour of the Greenland Ice Sheet, and the processes responsible for the ice sheet's evolution.

6.1 Decadal variability of Arctic sea ice

Satellites have observed a decline in Arctic sea ice extent for all months since 1979, coincident with abrupt global and Arctic warming over the last 30 years (Hartmann et al., 2013). The decline in Arctic sea ice extent is strongest in September, when Arctic sea ice extent reaches its annual minimum. September sea ice extent decreased by 13% decade^{-1} from 1979-2016, resulting in a record minimum ice extent of 3.41 million km^2 on September 16th 2012 (Fetterer et al., 2002, updated daily). The ten lowest minimum Arctic sea ice extents on satellite record have all occurred since 2005.

Further insight into changes in Arctic-wide and regional sea ice cover can be gained from mapping recent annual anomalies in ice concentration relative to decadal means (Figure 15). In spring (March/April; towards the end of the sea ice growth season) 2016, there was little difference in the concentration of sea ice in the central Arctic compared with the 2005-2016 mean. However, there were significant differences in springtime ice concentration in the more southerly regions

646 that have a predominantly seasonal, first year ice (FYI) cover. Within the Atlantic sector (defined as
647 the area encompassing the Greenland Sea, Iceland Sea, Barents Sea, Kara Sea, White Sea, Labrador
648 Sea, and Gulf of St Lawrence/Nova Scotia peninsula) the 2016 ice concentration was anomalously
649 low in the Greenland, Iceland and Barents Seas but higher in the western Labrador Sea and Gulf of
650 St Lawrence, and along the Nova Scotia peninsula. In autumn (October/November; the period
651 following the annual minimum sea ice extent) 2016 Arctic-wide sea ice concentration was ~15%
652 lower than the 2005-2016 mean, coincident with the decline observed in Arctic-wide sea ice
653 extent. The greatest anomalous lows occurred in the Iceland and Kara Seas, which are seasonal
654 regions that fall within the Atlantic sector.
655
656 Sea ice concentration has also exhibited large inter-annual variability in recent years. Within the
657 Atlantic Sector, and indeed the wider Arctic, 2016 was an unusual year. At the end of March 2016,
658 sea ice extent was below average in most of the seasonal regions, most notably in the Barents and
659 Kara seas, but not the Labrador Sea. These variations were associated with anomalously warm
660 conditions over the Arctic Ocean, driven by a pattern of above-average sea level pressures centred
661 over the ocean north of Alaska, and below-average pressures over the Atlantic side of the Arctic
662 (NOAA, 2016). In addition, the Barents and Kara seas were experiencing an influx of warm Atlantic
663 waters (NSIDC, 2016a). The autumn of 2016 was associated with unusually slow growth of sea ice
664 following the annual minimum extent, and in the Kara Sea it has been suggested that the slow ice
665 growth was due to above average sea surface temperatures for the time of year (NSIDC, 2016b).
666
667 **6.2 Importance of Arctic sea ice thickness and volume observations**
668 Arctic-wide observations of sea ice concentration have provided insight into decadal-scale changes

669 in the ice cover. However, to fully understand regional and global impacts of these changes, long-
670 term, accurate estimates of total ice volume are required. Sea ice thickness and volume estimates
671 can be obtained from some models, such as the Pan-Arctic Ice-Ocean Modelling and Assimilation
672 System (PIOMAS, Zhang and Rothrock, 2003). From an observational perspective, the European
673 Space Agency's (ESA's) CryoSat-2 satellite (Wingham et al., 2006) provides unparalleled coverage
674 of the Arctic Ocean up to 88°N since 2010. CryoSat-2 data have been used to produce the first
675 observational estimates of sea ice thickness and volume across the entire Northern Hemisphere
676 over the sea ice growth season, before melt ponds begin to form on the ice (Tilling et al., 2016;
677 Tilling et al., 2015).
678
679 Since 1980, PIOMAS shows a decline in Arctic sea ice volume for autumn of 16% decade^{-1} and a
680 decline in spring volume of 8% decade^{-1} (Figure 16). Since 2005 the decline in autumn volume has
681 increased to 25% decade^{-1} whereas the decline in spring volume has remained more stable at 9%
682 decade^{-1}. Over the CryoSat-2 period alone there have been clear seasonal and inter-annual
683 variations in the volume of Northern Hemisphere sea ice cover. For example, between 2010-2016,
684 the large (349 to 468 km^3 yr^{-1}) inter-annual fluctuations in ice volume (Figure 16) were two to
685 three times greater than the variability that occurred in the central Arctic between 2003 and 2008
686 (115 to 275 km^3 yr^{-1}) – the only other period for which satellite observations of Arctic sea ice
687 volume exist (Kwok et al., 2009). For the CryoSat-2 period, the Atlantic sector contributed 9% and
688 14% to the total autumn and spring sea ice volume, respectively. Total autumn sea ice volume
689 declined by 14% (1,279 km^3) between 2010 and 2012, increased by 41% (3,184 km^3) in 2013, and
690 then decreased by 22% (2,629 km^3) between 2013 and 2016. The peak autumn volume in 2013
691 was associated with the retention of thick ice in the multi-year ice region north of Greenland and

692 Ellesmere Island coincident with a ~5% drop in the number of days on which melting occurred
693 over summer. The sharp increase in sea ice volume after just one cool summer demonstrates the
694 ability of Arctic sea ice to respond rapidly to a changing environment (Tilling et al., 2015).
695
696 **6.3 Recent changes in the mass of the Greenland Ice Sheet**
697 Since the early 1990s, mass loss from the Greenland Ice Sheet has contributed approximately 10%
698 of the observed global mean sea level rise (Vaughan et al., 2013). During this period, the ice
699 imbalance has progressively increased with time (Rignot et al., 2011; Shepherd et al., 2012), from
700 34 ± 40 Gt yr^{-1} between 1992 and 2001, to 215 ± 59 Gt yr^{-1} between 2002 and 2011 (Vaughan et
701 al., 2013), and to 269 ± 51 Gt yr^{-1} between 2011 and 2014. The latter rate corresponds to an
702 annual contribution of 0.74 ± 0.14 mm yr^{-1} to global mean sea level (McMillan et al., 2016).
703 Regionally, Greenland's South West has experienced the greatest loss of ice (Figure 17),
704 contributing ~ 40 % of the total ice sheet imbalance between 2011-2014 (McMillan et al., 2016). In
705 contrast, the North East sector contributed ~ 10 % of ice losses, with the remainder split almost
706 equally between the South East and North West sectors (Figure 17).
707
708 Satellite, airborne and field observations show that ice loss has been predominantly focussed upon
709 ice margin regions and marine terminating outlet glaciers (Enderlin et al., 2014; Joughin et al.,
710 2014; Rignot et al., 2010; Thomas et al., 2006), which are sensitive to warming at their
711 atmospheric and ocean interfaces. Inland, within the cooler, slow-flowing interior, and particularly
712 at more southerly latitudes, snowfall driven mass accumulation occurred throughout the 1990s
713 and up to 2005 (Thomas et al., 2006). However, since 2005 inland snowfall, and associated mass
714 gains, appear to have diminished (Kuipers Munneke et al., 2015). Over shorter, inter-annual

timescales, Greenland's mass balance has fluctuated considerably (Figure 17). In 2012, for example, a record mass deficit of 439 ± 62 Gt was recorded, only to be followed in 2013 by losses 116 ± 65 Gt in 2013, which were approximately half the decadal mean (McMillan et al., 2016). At the finer scale of individual glacier systems, the spatial and temporal pattern of variability is also complex, with glacier response to changes in ocean (Holland et al., 2008) and atmospheric (Fettweis et al., 2011) forcing being modulated by both glacier geometry and setting.

6.4 Drivers of recent changes in the mass of the Greenland Ice Sheet.

Recent fluctuations in Greenland Ice Sheet mass have been driven by two processes; changing surface mass balance and variable glacier flow. Between 2000 and 2008 ice loss was due, in almost equal amounts, to decreased surface mass balance and increased ice discharge (van den Broeke et al., 2009). These changes were driven by a combination of warmer summer temperatures (Fettweis et al., 2013), and glacier flow acceleration across much of the South East and North West sectors (Enderlin et al., 2014).

Since 2008, several exceptionally warm summers have produced episodes of widespread surface melt (Fettweis et al., 2013; Nghiem et al., 2012), which has been particularly intense along the western margin of the ice sheet (Hanna et al., 2012). 2012, in particular, was notable for unprecedented surface melting across almost the entire ice sheet (Nghiem et al., 2012). Intense melt events such as these have been linked to the advection of warmer southerly air over the ice sheet, driven by persistent high pressure systems associated with a strong negative phase of the North Atlantic Oscillation (NAO) and a high Greenland Blocking Index (Hanna et al., 2014). In contrast, 2013 saw low-pressure and low-temperature conditions, coinciding with the most

positive summertime NAO recorded in the past 20 years, and unusually low ice mass loss. Together, these contrasting years illustrate the recent sensitivity of Greenland ice mass balance to large scale modes of atmospheric variability, with intense melt events lasting only a few months capable of making relatively large contributions to multi-year ice mass balance.

7. Synthesis and Discussion

This report has brought together an unprecedented range of evidence about recent changes in the North Atlantic Climate System. It documents trends in atmospheric circulation and composition, in ocean circulation and properties, and in the cryosphere, with a primary focus on the period since 2000 and especially since 2005. Focussing on the period since 2005, some of the major trends identified and discussed include:

- An increase in the speed of the North Atlantic jet stream in winter (Fig 2a) associated with an increase in sea level pressure across the mid-latitude Atlantic and a decrease in the northeast Atlantic (Fig 3b).
- Increases in ozone and methane (Figs 6 and 7)
- Increases in net absorbed radiation in the mid-latitude western Atlantic, which correlate with an increase in the abundance of high-level clouds and a reduction in low-level clouds (Fig 10).
- Cooling of sea surface temperatures (SST) in the subpolar gyre, concomitant with increases in the western subtropical gyre, and a decline in the Atlantic overturning circulation (Figs 13 & 14)

- A decline in Atlantic sector Arctic sea-ice and increased rates of melting of the Greenland Ice Sheet (Figs 16 and 17)

The report raises many questions about the significance and causes of the various trends, and – implicitly – the extent to which they may continue in future, or change. The report is structured around the different components of the North Atlantic Climate System but a fundamental point is that the trends in these different components are not independent. There are many exchange processes that link the different variables, and understanding the relative importance of different processes is an important challenge. Some examples of the linkage questions raised by this report are:

- What have been the roles of atmospheric circulation and composition in driving the trends in ocean circulation and properties?
- To what extent have the changes in atmospheric circulation been influenced by the changes in SST?
- What has been the role of atmospheric circulation, including the NAO, in shaping the trends in ozone and methane?
- To what extent have the changes in clouds and net absorbed radiation been a factor in the (similarly located) warming of SST in the western subtropical gyre? And to what extent have the SST trends influenced the clouds?
- What has been the role of atmosphere and ocean circulation in driving the trends observed in Atlantic sector Sea Ice and Greenland Ice Sheet mass?

Maintaining and expanding the observational capacity in the North Atlantic and continuing in-depth process based analysis of observations and models is crucial to unravel these linkages.

Acknowledgments

This review article was written with support of the NERC North Atlantic Climate System: integrated Study (ACSIS) project.

Figures

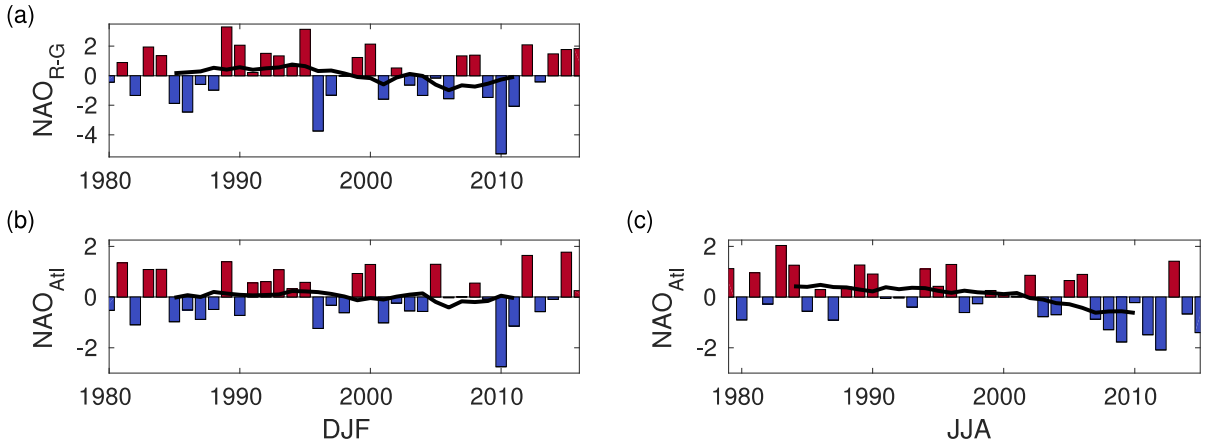

***Figure 1**: (a) NAO index estimated from the normalised difference of surface pressures at Reykjavik and Gibraltar. Each of the surface pressure time series are normalised by their respective standard deviations, so the index is dimensionless. (b) DJF Atlantic NAO index estimated as the surface pressure principal component time series over the region 60-0°W, 30-70°N. The principal component time series is normalised by its standard deviation, so the index is dimensionless. (c) JJA Atlantic NAO index otherwise as (b). All plots: the bars indicate the seasonal mean values and the thick black line indicates an 11-year running mean.*

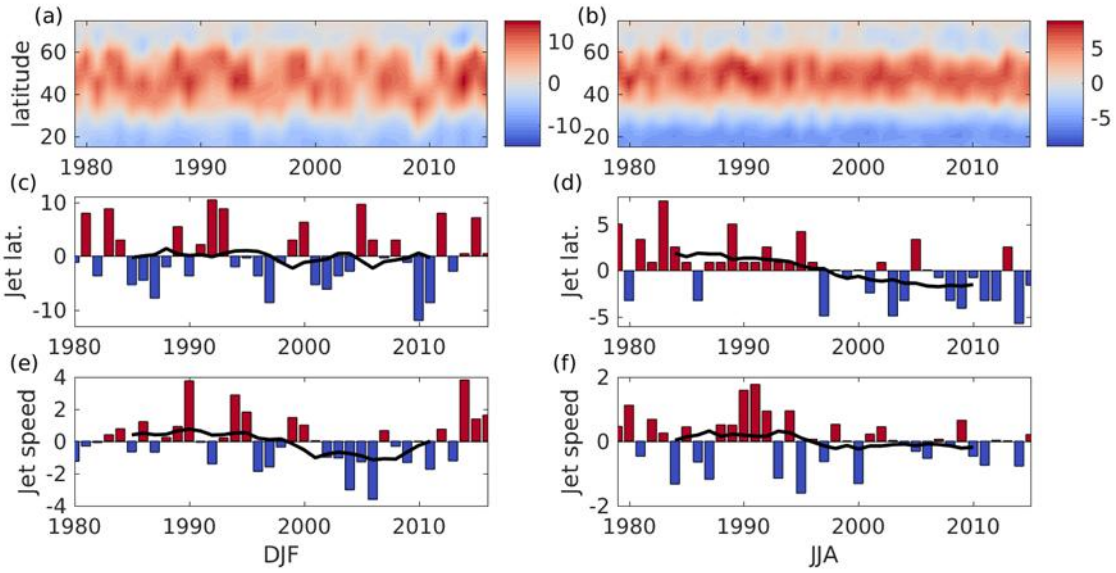

Figure 2: *Top row: (a) and (b), seasonal and longitudinal average of the zonal velocity as a function of latitude at 850 hPa in the region 60-0°W, (m/s). Note the change in colour scale. Middle row: (c) and (d), latitude anomaly (degrees) of the maximum of the seasonal mean zonal velocity at 850 hPa in the region 60-0°W, 15-75°N. Bottom row: (e) and (f), anomaly of the maximum of the seasonal mean zonal velocity (m/s) at 850 hPa in the region 60-0°W, 15-75°N. Left: index averaged over DJF. Right: index averaged over JJA. All plots: the bars indicate the monthly mean values and the thick black line indicates an 11-year running mean.*

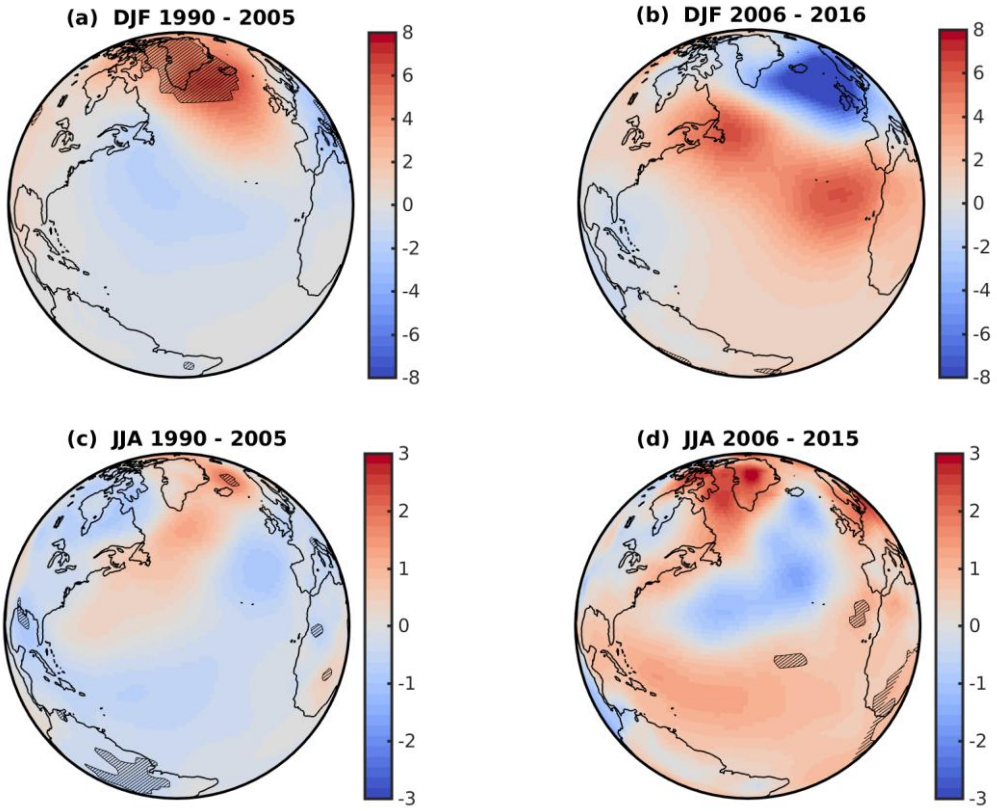

***Figure 3**: Trends in the seasonal mean surface pressure in hPa per decade. Hatched regions are where the trend exceeds the 95% confidence interval for Gaussian distributed random numbers, with one number per season.*

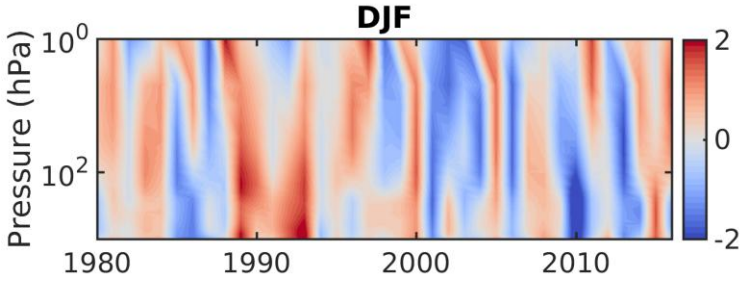

***Figure 4**: Seasonal average of the DJF zonal mean zonal wind anomaly at 60N (m/s). The time series on each pressure level has been normalised to have a standard deviation of one in order to highlight the barotropic nature of the flow.*

804

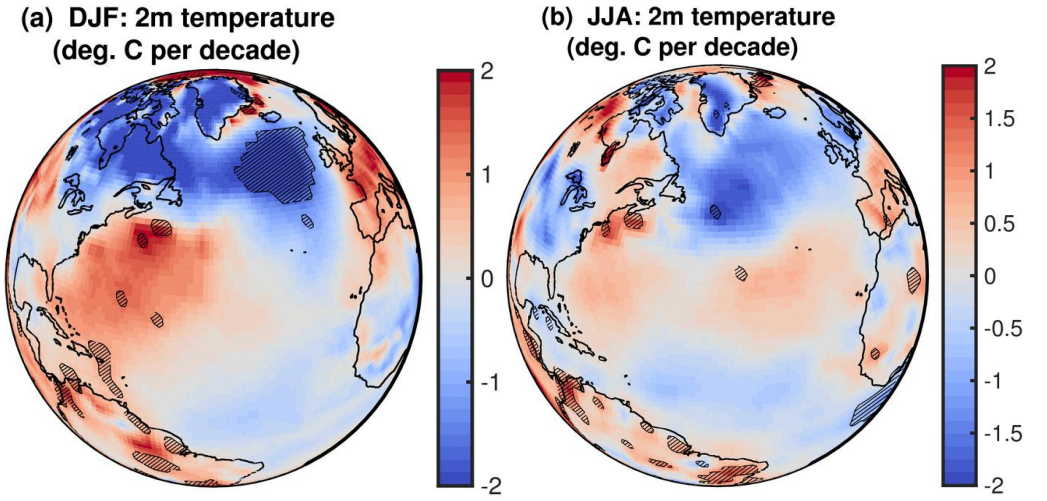
(a) DJF: 2m temperature
(deg. C per decade)
2
1
0
-1
-2
(b) JJA: 2m temperature
(deg. C per decade)
2
1.5
1
0.5
0
-0.5
-1
-1.5
-2

805

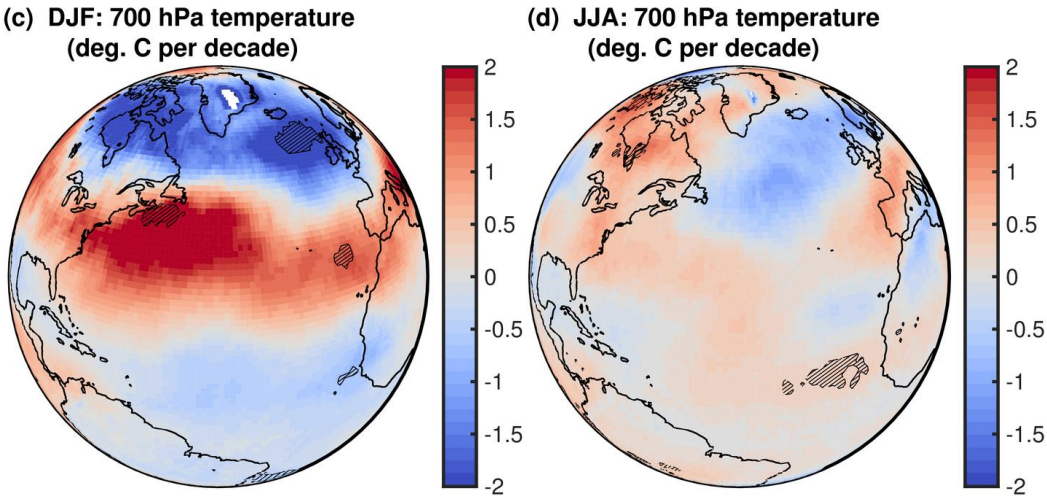
(c) DJF: 700 hPa temperature
(deg. C per decade)
2
1.5
1
0.5
0
-0.5
-1
-1.5
-2
(d) JJA: 700 hPa temperature
(deg. C per decade)
2
1.5
1
0.5
0
-0.5
-1
-1.5
-2

806

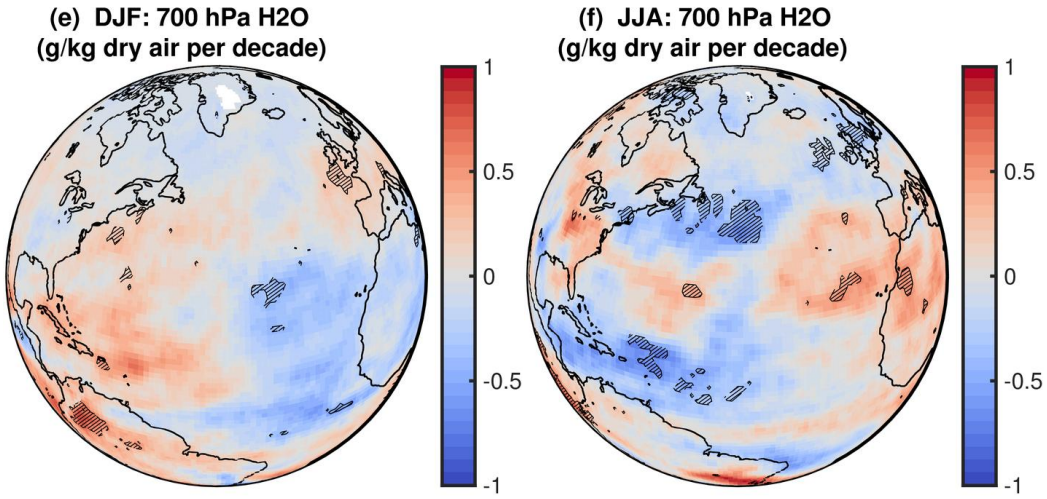
(e) DJF: 700 hPa H2O
(g/kg dry air per decade)
1
0.5
0
-0.5
-1
(f) JJA: 700 hPa H2O
(g/kg dry air per decade)
1
0.5
0
-0.5
-1

807

***Figure 5**: Decadal trends over the period 2006-2016. Top row: (a) and (b), 2m air temperature trend using ERA-interim data. Middle row: (c) and (d), 700 hPa temperature, as measured by AIRS, see http://airs.jpl.nasa.gov. Bottom row: (e) and (f), 700 hPa water mass mixing ratio, as measured by AIRS.*

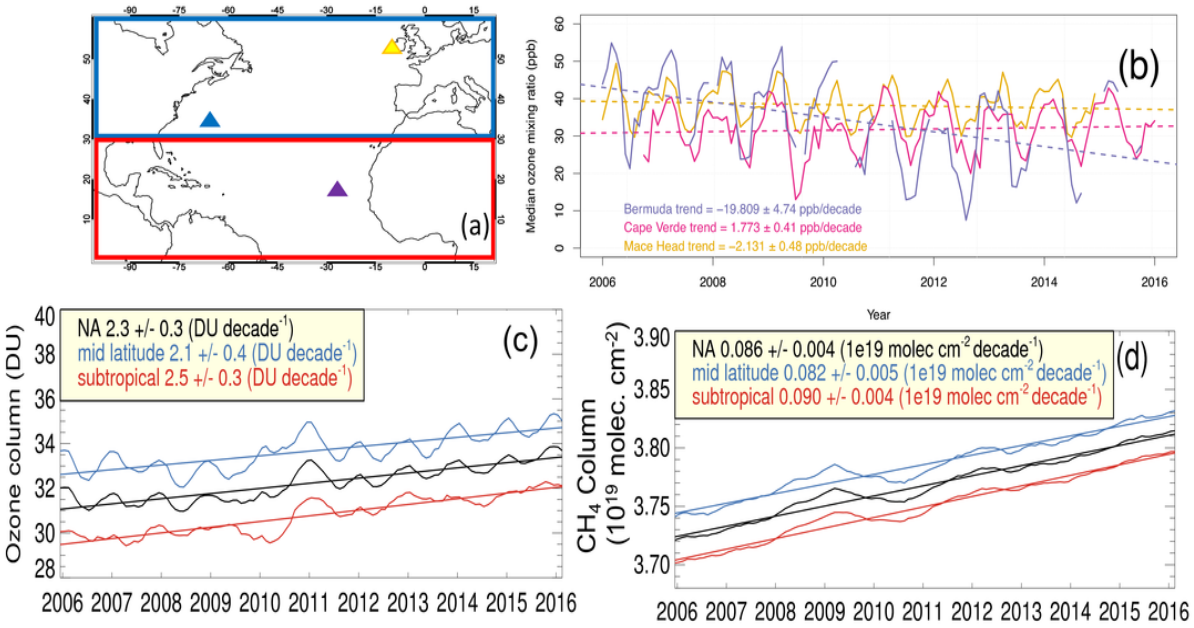

***Figure 6**: Timeseries from satellite and surface in situ measurements in the North Atlantic. Monthly median surface ozone mixing ratios (panel b) are shown for three long-term monitoring sites in the North Atlantic: Bermuda (64.87E; 32.31N), Cape Verde (24.87E; 16.54N), Mace Head (9.90E; 53.32N) (locations shown as triangles in panel a). Satellite trends (panels c-d) are calculated over the period 12/2005-2/2016 (123 months) for average values over 3 domains: North Atlantic (100°W-20°E; 0:60°N), mid latitude (100°W-20°E; 30-60°N), subtropical (100°W-20°E; 0:30°N). The curves plotted are 12 months running averages. Tropospheric ozone column trends from monthly*

821 *OMI-MLS data; methane column trends from AIRS; surface in situ measurements from Global*

822 *Atmospheric Watch.*

823

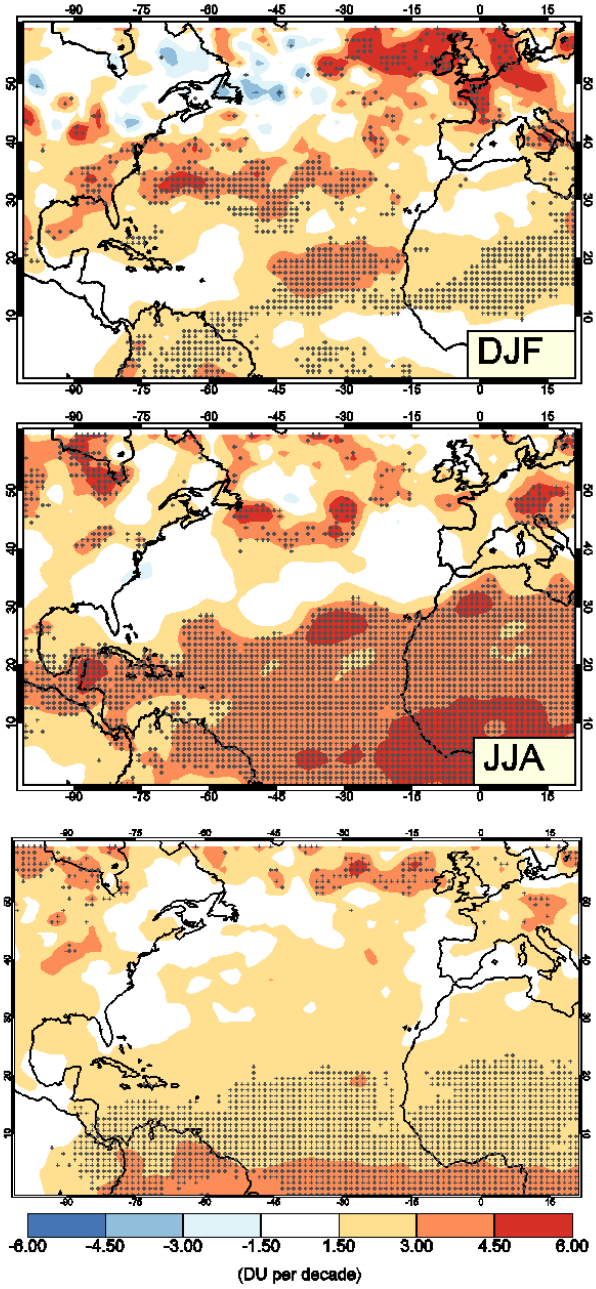

824

825 ***Figure 7:*** *Decadal linear trends (ca. 2006-2016) calculated using seasonal (DJF (top) and JJA*

826 *(middle)) and annual-mean (bottom) ozone tropospheric column. Trends are calculated over the*

period 12/2005-2/2016. The stippling indicates where trends are significant to the 95% confidence level, based on the standard error of the residuals (Wigley et al., 2006) *. Methane trends show little variation spatially and seasonally (not shown).*

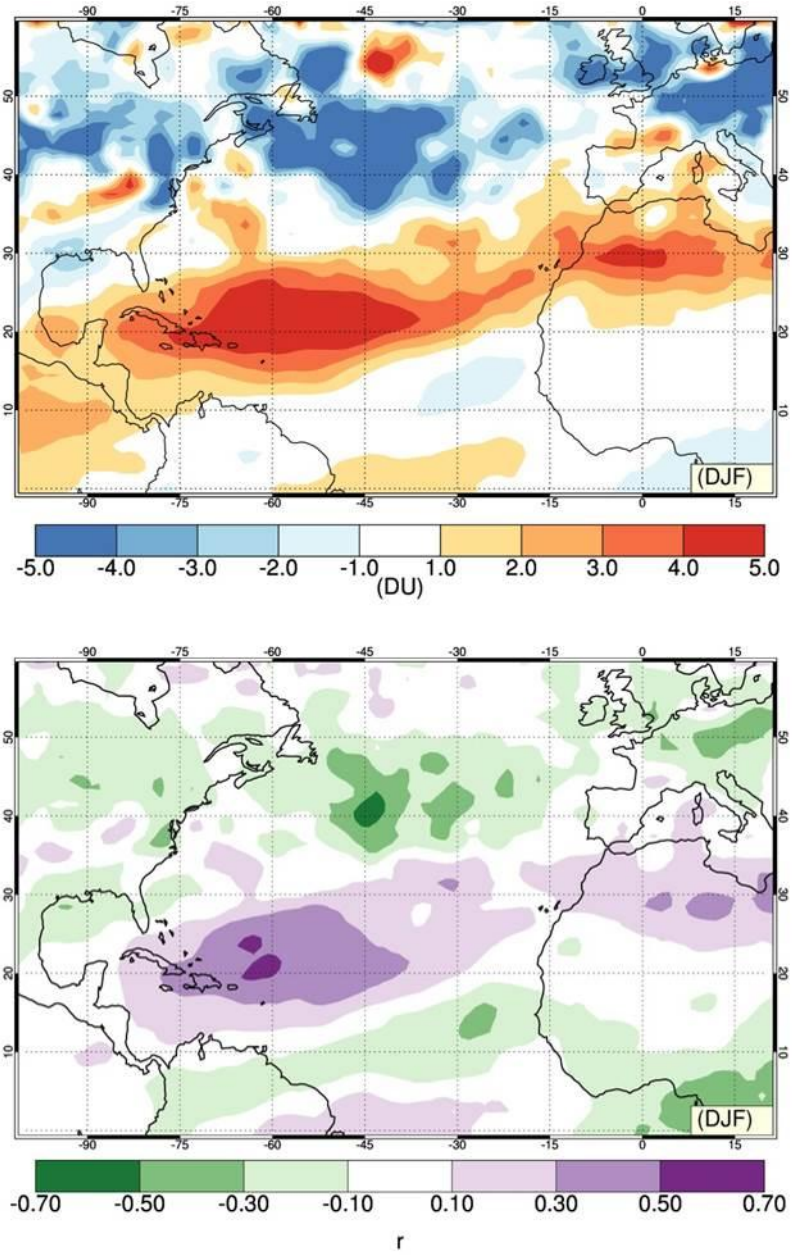

Figure 8: *Impacts of NAO on tropospheric ozone column. Top panel shows difference in mean ozone tropospheric column between winter months with 'high' and 'low' NAO indices (high/low are*

defined as months between 12-2005 and 2-2016 with NAO index greater/smaller than +/-2). Bottom panel shows the correlation coefficient between tropospheric ozone column at each location and winter months NAO indices. NAO index is calculated as the difference between the normalised sea level pressure over Gibraltar and the normalised sea level pressure over Southwest Iceland (Jones et al., 1997). *Ozone data is detrended prior to the analysis.*

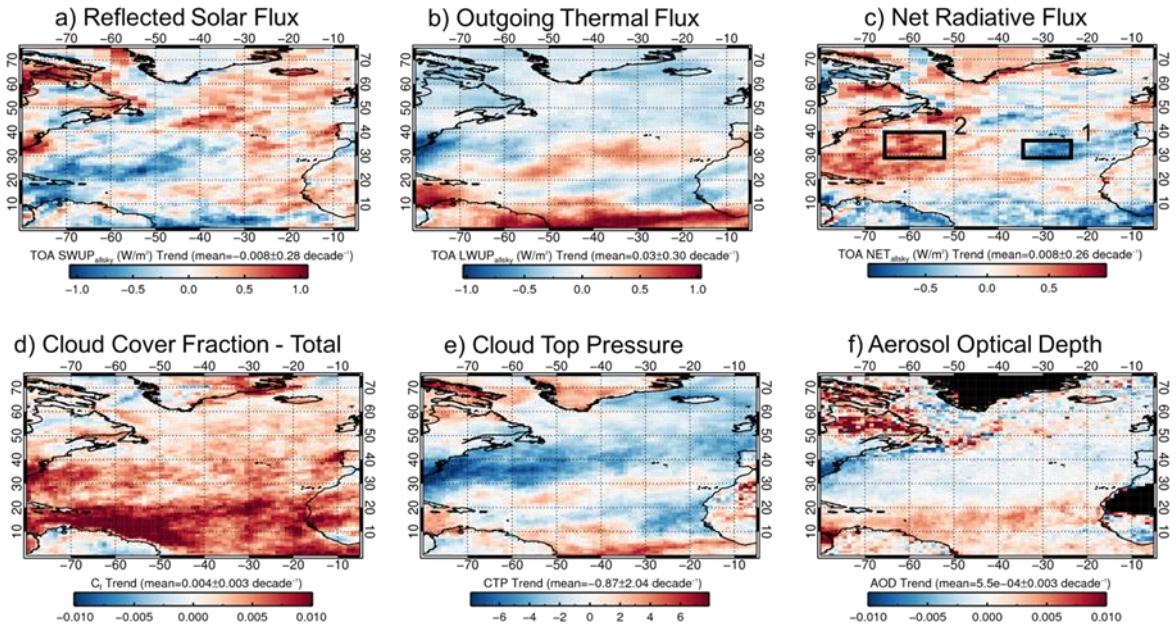

Figure 9*. Trends in the anomalies computed from the monthly mean top of atmosphere a) outgoing shortwave, b) outgoing longwave, and c) net radiative flux computed using allsky monthly mean CERES-EBAF during the period 2006 – 2016 over the North Atlantic region (note positive is a net downward flux in c). The MODIS MOD08_M3 product also displays d) allsky cloud cover fraction, e) cloud top pressure, and f) aerosol optical depth. Trends are computed using the period 2006 – 2016 over the North Atlantic region. Two boxes are displayed showing regions with substantial cooling (box 1 in the East Atlantic) and warming (box 2 in the West Atlantic). Mean*

trends of the anomalies are reported as a change per decade. Regions in black contain missing data.

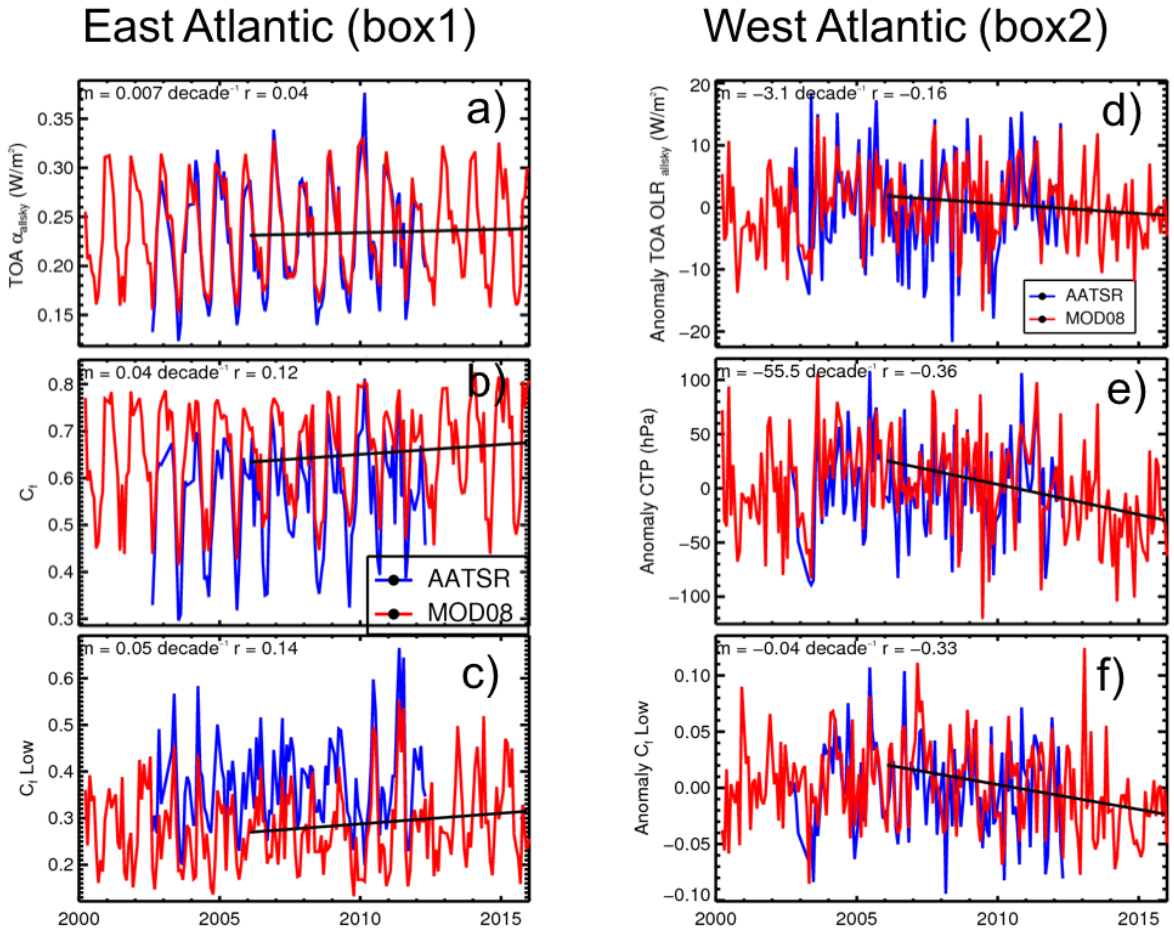

Figure 10*. Monthly averages of a) top of atmosphere allsky albedo, b) total cloud fraction, and c) low-level cloud fraction defined as a cloud top pressure greater than 500 hPa for the observations in the East Atlantic region (box 1). Monthly anomalies of d) top of atmosphere outgoing long wave flux, e) cloud top pressure, and f) low-level cloud fraction. MODIS (red line) and AATSR (blue line) data sets are shown and the trend is computed over MODIS observations from 2006—2016.*

Anomalies (right panel only) are computed using the 2002-2012 period from independent

retrievals from AATSR and MODIS observations. The slope (m) and correlation coefficient (r) are provided for each time series.

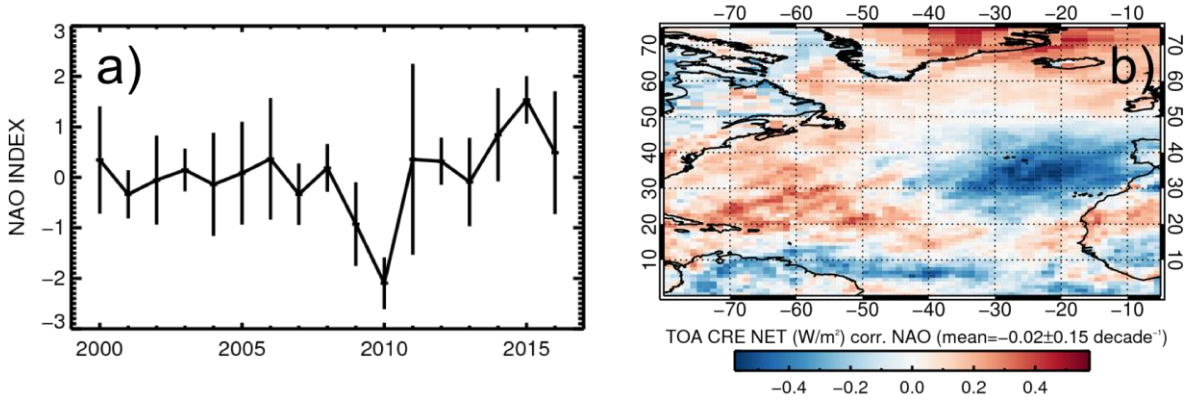

Figure 11*. a) North Atlantic Oscillation (NAO) index averaged over December, January, February (DJF) months* (Hurrell, 1995) *and b) correlation of the observed cloud radiative effect (CERES) with the NAO index over the period from 2000 - 2016.*

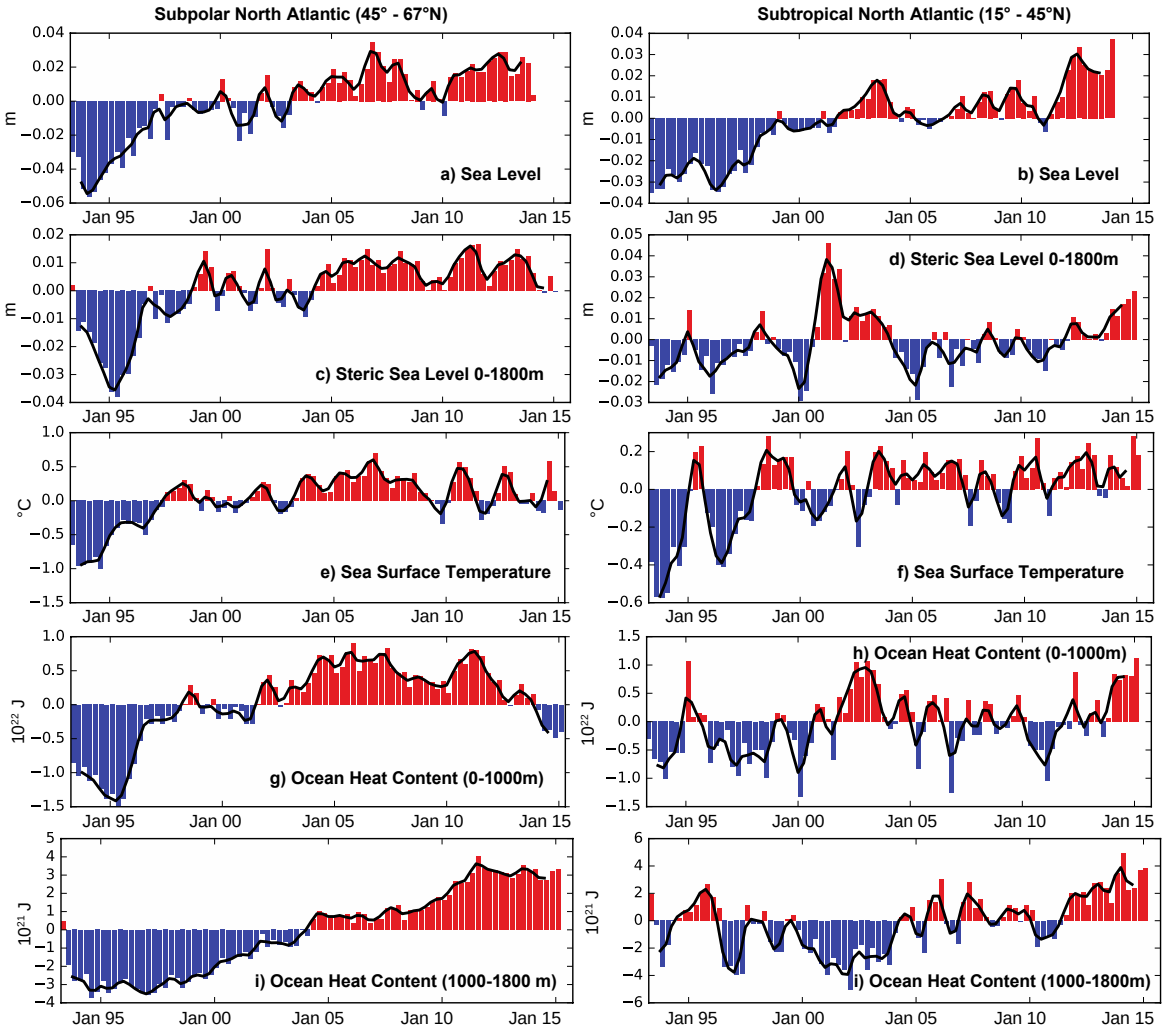

Figure 12. *Time series of North Atlantic subpolar (left column) and subtropical (right column) sea level, sea surface temperature and ocean heat content anomalies. (**a-b**) are sea level change (m), and (**c-d**) are steric sea level change (m), all anomalies from 1993-2014 mean seasonal means. (**e-f**) are sea surface temperature (SST) anomalies from the 1993-2014 seasonal means. (**g-h**) are 0-1000m ocean heat content anomaly from 1993-2015 seasonal mean, and (**i-j**) are same except 1000-1800m. Sea Level and SST data are from the ESA Climate Change Initiative project (Hollmann*

873 *et al. 2013; Merchant et al. 2014; Ablain et al. 2015, 2017). Heat content anomalies derived from*

874 *EN4 datasets* (Good et al., 2013) *(www.metoffice.gov.uk/hadobs/en4/).*

875

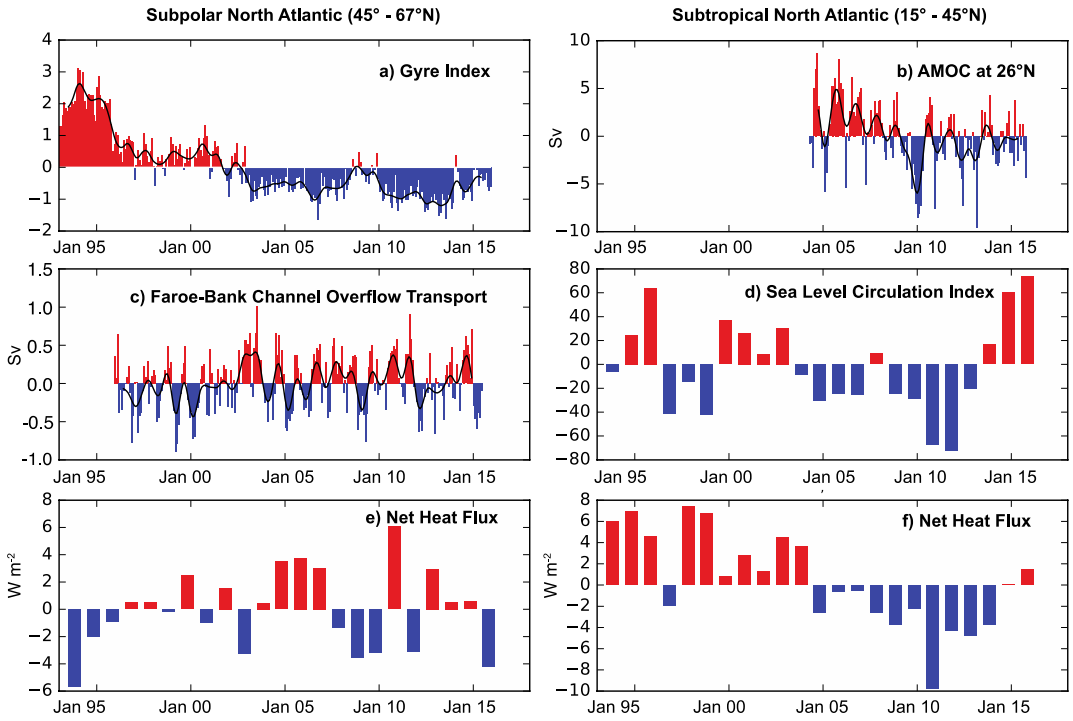

876

877 ***Figure 13****. Time series of North Atlantic ocean circulation and air-sea heat flux anomalies. (a) A*

878 *subpolar gyre circulation index derived from ESA Climate Change Initiative sea level product*

879 *(principle component of first EOF of SPNA sea surface height). (b) The meridional overturning*

880 *circulation observed at 26°N by the RAPID array (www.rapid.ac.uk). (c) The transport of overflow*

881 *water at the Faroe Bank Channel (after Hansen et al, 2016). (d) A subtropical-to-subpolar circulation*

882 *index derived from sea-level gradient along the east coast of North America (after* McCarthy et al.,

883 2015). *(e-f) Net heat flux derived from ERA-Interim reanalysis data product. All anomalies are from*

884 *1993-2015 mean, or full time series length if shorter.*

885

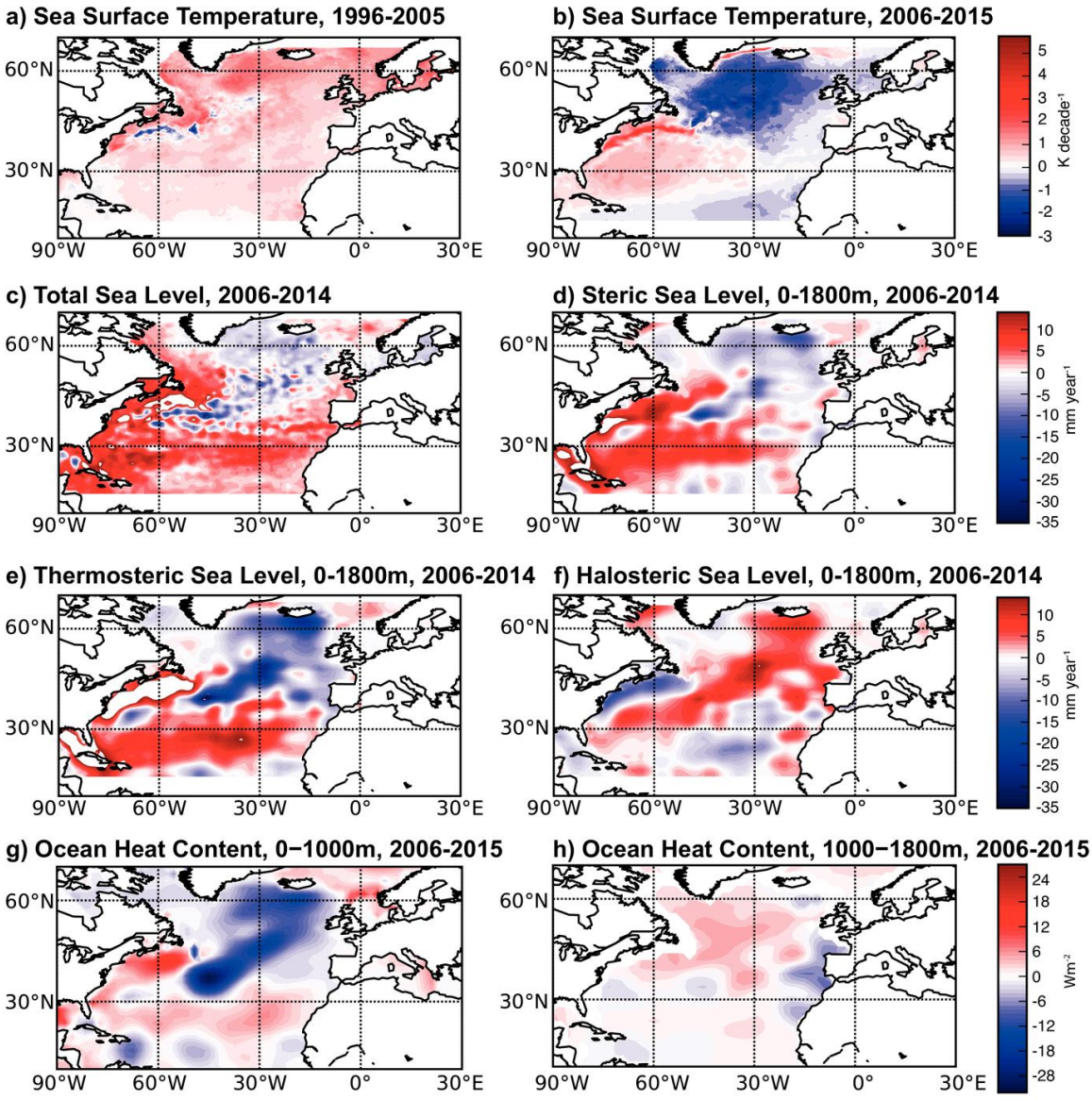

886

887 *Figure 14. Recent decadal trends of key North Atlantic ocean variables. (a) Sea surface temperature*

888 *trend for 1996 to 2005. (b) Sea surface temperature trend for 2006 to 2015. (c) Sea level trend for*

889 *2006 to 2014. (d) Total steric sea level trend (0-1800m) for 2006 to 2014. (e) Thermosteric sea level*

890 *trend (0-1800m) for 2006 to 2014. (f) Halosteric sea level trend (0-1800m) for 2006 to 2014. (g)*

891 *Ocean heat content trend for 2006-2016 (0-1000m). (h) Ocean heat content trend for 2006-2016*

(1000-1800m). Sea Level and SST data are from the ESA Climate Change Initiative project. Heat content, steric, thermostreic and halosteric anomalies derived from EN4 dataset.

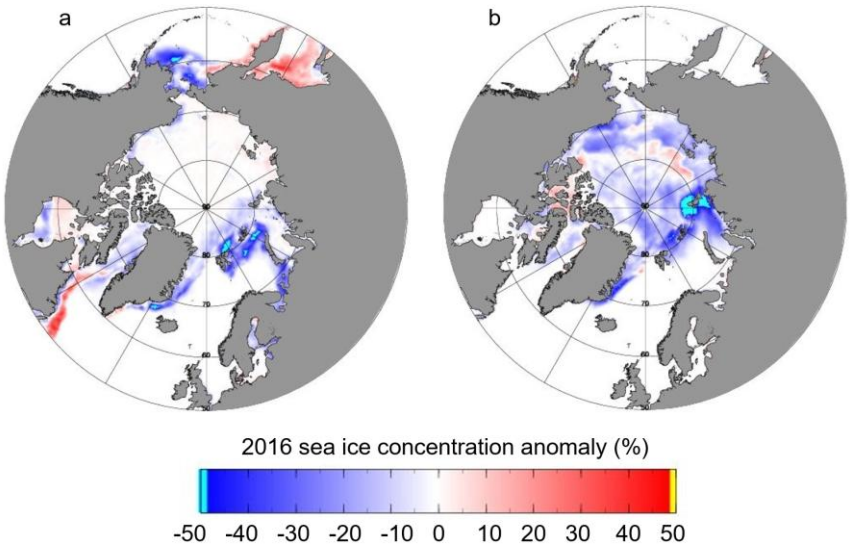

Figure 15: *Arctic sea ice concentration anomaly in 2016, relative to the 2005-2016 mean, for (a) spring (March/April) and (b) autumn (October/November), from PIOMAS. Regions with a mean sea ice concentration less than 5% are not shown, and the extent is masked for 2016.*

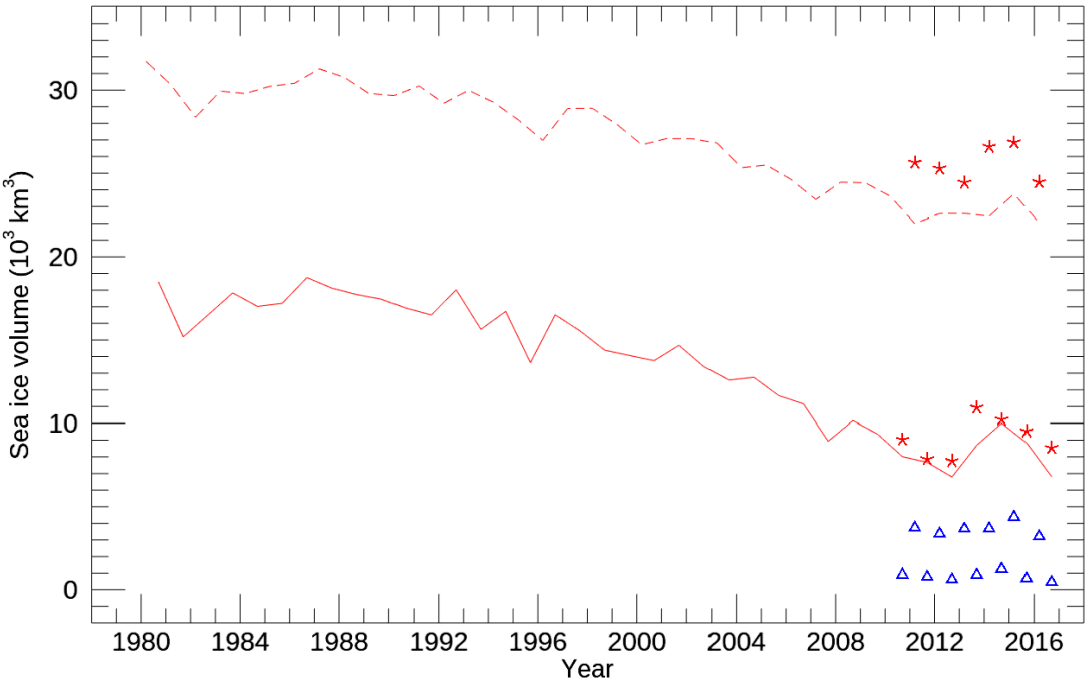

902

903 ***Figure 16:*** *Time series of PIOMAS model Arctic sea ice volume for autumn 1980–2015 (solid line)*

904 *and spring 1980–2016 (dashed line). CryoSat-2 volume estimates are plotted for autumn*

905 *(October/November) 2010–2014 and spring (March/April) 2011-2014, Arctic-wide (red stars) and*

906 *within the Atlantic sector (blue triangles).*

907

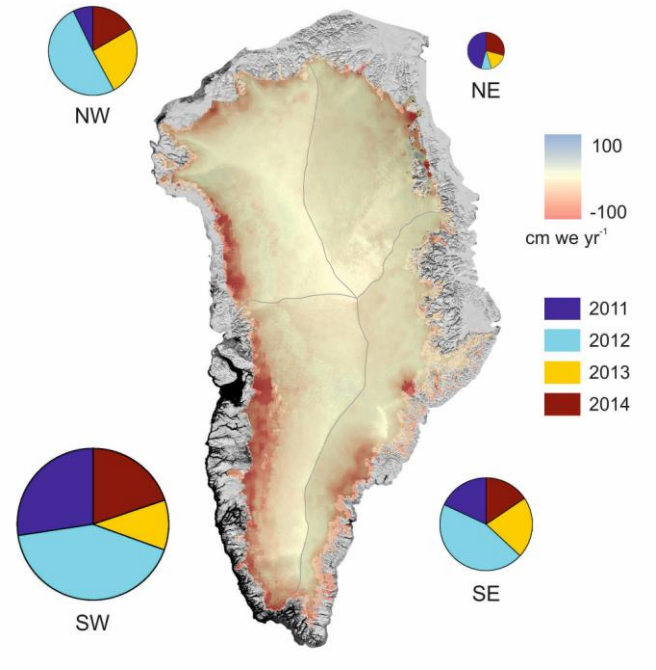

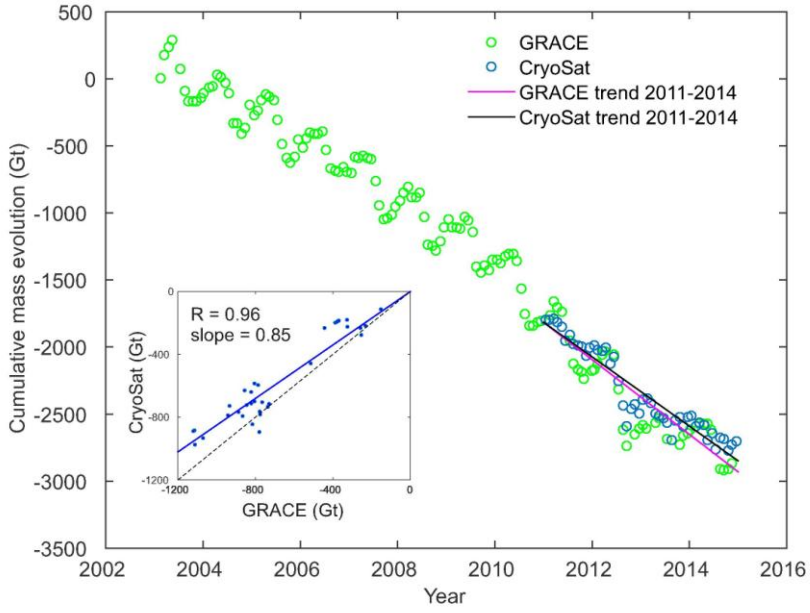

Figure 17: *Top panel. Rate of mass change of the Greenland Ice Sheet between January 2011 and December 2014. For each of the southwest (SW), southeast (SE), northeast (NE) and northwest (NW) sectors, the colour wheel indicates the proportion of mass lost in each year, with the radius*

scaled according to the magnitude of the total losses. The boundaries between the four sectors are shown in grey. Bottom panel. Monthly evolution in ice sheet mass since 2003 from GRACE gravimetry (green) and since 2011 from CryoSat-2 altimetry and firn modelling (blue). The CryoSat-2 time-series has been referenced to the GRACE data at the start of 2011. The inset shows the correspondence between the GRACE and CryoSat-2 monthly estimates of mass evolution since 2011 (solid blue dots), together with a linear regression (solid blue line), the regression slope and the Pearson correlation coefficient, R. The dashed line indicates equivalence, although the GRACE results include, additionally, mass changes of peripheral ice caps and unglaciated regions (McMillan et al., 2016).

References

Atkinson, J.D., Murray, B.J., Woodhouse, M.T., Whale, T.F., Baustian, K.J., Carslaw, K.S., Dobbie, S., O'Sullivan, D., Malkin, T.L., 2013. The importance of feldspar for ice nucleation by mineral dust in mixed-phase clouds. Nature 498, 355–358. https://doi.org/10.1038/nature12278

Ba, J., Keenlyside, N.S., Latif, M., Park, W., Ding, H., Lohmann, K., Mignot, J., Menary, M., Otterå, O.H., Wouters, B., Melia, D.S. y, Oka, A., Bellucci, A., Volodin, E., 2014. A multi-model comparison of Atlantic multidecadal variability. Clim. Dyn. 43, 2333–2348. https://doi.org/10.1007/s00382-014-2056-1

Bacer, S., Christoudias, T., Pozzer, A., 2016. Projection of North Atlantic Oscillation and its effect on tracer transport. Atmospheric Chem. Phys. 16, 15581–15592. https://doi.org/10.5194/acp-16-15581-2016

Baehr, J., Haak, H., Alderson, S., Cunningham, S.A., Jungclaus, J.H., Marotzke, J., 2007. Timely Detection of Changes in the Meridional Overturning Circulation at 26°N in the Atlantic. J. Clim. 20, 5827–5841. https://doi.org/10.1175/2007JCLI1686.1

Bell, C.J., Gray, L.J., Charlton-Perez, A.J., Joshi, M.M., Scaife, A.A., 2009. Stratospheric Communication of El Niño Teleconnections to European Winter. J. Clim. 22, 4083–4096. https://doi.org/10.1175/2009JCLI2717.1

Berx, B., Payne, M.R., 2016. The Sub-Polar Gyre Index – a community data set for application in fisheries and environment research. Earth Syst. Sci. Data Discuss. 1–15. https://doi.org/10.5194/essd-2016-53

Biastoch, A., Böning, C.W., Lutjeharms, J.R.E., 2008. Agulhas leakage dynamics affects decadal variability in Atlantic overturning circulation. Nature 456, 489–492. https://doi.org/10.1038/nature07426

Bingham, R.J., Hughes, C.W., Roussenov, V., Williams, R.G., 2007. Meridional coherence of the North Atlantic meridional overturning circulation: MERIDIONAL COHERENCE OF ATLANTIC MOC. Geophys. Res. Lett. 34, n/a-n/a. https://doi.org/10.1029/2007GL031731

Blaker, A.T., Hirschi, J.J.-M., McCarthy, G., Sinha, B., Taws, S., Marsh, R., Coward, A., de Cuevas, B., 2015. Historical analogues of the recent extreme minima observed in the Atlantic meridional overturning circulation at 26 N. Clim. Dyn. 44, 457–473.

Booth, B.B.B., Dunstone, N.J., Halloran, P.R., Andrews, T., Bellouin, N., 2012. Aerosols implicated as a prime driver of twentieth-century North Atlantic climate variability. Nature 484, 228–232. https://doi.org/10.1038/nature10946

Bower, A.S., Lozier, M.S., Gary, S.F., Böning, C.W., 2009. Interior pathways of the North Atlantic meridional overturning circulation. Nature 459, 243–247. https://doi.org/10.1038/nature07979

Bryden, H.L., Imawaki, S., 2001. Chapter 6.1 Ocean heat transport. Int. Geophys., Ocean Circulation and Climate 77, 455–474. https://doi.org/10.1016/S0074-6142(01)80134-0

Buckley, M.W., Marshall, J., 2016. Observations, inferences, and mechanisms of the Atlantic Meridional Overturning Circulation: A review. Rev. Geophys. 54, 2015RG000493. https://doi.org/10.1002/2015RG000493

Cattiaux, J., Vautard, R., Cassou, C., Yiou, P., Masson-Delmotte, V., Codron, F., 2010. Winter 2010 in Europe: A cold extreme in a warming climate. Geophys. Res. Lett. 37, L20704. https://doi.org/10.1029/2010GL044613

Christensen, M.C., Poulsen, C., McGarragh, G., Grainger, R., 2016. Algorithm Theoretical Basis Document (ATMD) of the Community Code for CLimate (CC4CL) Broadband Radiative Flux Retrieval (CC4CL-TOAFLUX) module, Version 1.0 (Phase 2 ESA cloud_cci report for cloud option #4).

Cooper, O.R., Parrish, D.D., Ziemke, J., Balashov, N.V., Cupeiro, M., Galbally, I.E., Gilge, S., Horowitz, L., Jensen, N.R., Lamarque, J.-F., Naik, V., Oltmans, S.J., Schwab, J., Shindell, D.T., Thompson, A.M., Thouret, V., Wang, Y., Zbinden, R.M., 2014. Global distribution and trends of tropospheric ozone: An observation-based review. Elem. Sci. Anthr. 2, 000029. https://doi.org/10.12952/journal.elementa.000029

Creilson, J.K., Fishman, J., Wozniak, A.E., 2003. Intercontinental transport of tropospheric ozone: a study of its seasonal variability across the North Atlantic utilizing tropospheric ozone residuals and its relationship to the North Atlantic Oscillation. Atmospheric Chem. Phys. 3, 2053–2066. https://doi.org/10.5194/acp-3-2053-2003

Cunningham, S.A., Roberts, C.D., Frajka-Williams, E., Johns, W.E., Hobbs, W., Palmer, M.D., Rayner, D., Smeed, D.A., McCarthy, G., 2013. Atlantic Meridional Overturning Circulation slowdown cooled the subtropical ocean. Geophys. Res. Lett. 40, 6202–6207. https://doi.org/10.1002/2013GL058464

de Jong, M.F., de Steur, L., 2016. Strong winter cooling over the Irminger Sea in winter 2014-2015, exceptional deep convection, and the emergence of anomalously low SST. Geophys. Res. Lett. 43, 7106–7113. https://doi.org/10.1002/2016GL069596

Dee, D.P., Uppala, S.M., Simmons, A.J., Berrisford, P., Poli, P., Kobayashi, S., Andrae, U., Balmaseda, M.A., Balsamo, G., Bauer, P., Bechtold, P., Beljaars, A.C.M., van de Berg, L., Bidlot, J., Bormann, N., Delsol, C., Dragani, R., Fuentes, M., Geer, A.J., Haimberger, L., Healy, S.B., Hersbach, H., Hólm, E.V., Isaksen, L., Kållberg, P., Köhler, M., Matricardi, M., McNally, A.P., Monge-Sanz, B.M., Morcrette, J.-J., Park, B.-K., Peubey, C., de Rosnay, P., Tavolato, C., Thépaut, J.-N., Vitart, F., 2011. The ERA-Interim reanalysis: configuration and

performance of the data assimilation system. Q. J. R. Meteorol. Soc. 137, 553–597. https://doi.org/10.1002/qj.828

Desbruyères, D., McDonagh, E.L., King, B.A., Thierry, V., 2017. Global and Full-Depth Ocean Temperature Trends during the Early Twenty-First Century from Argo and Repeat Hydrography. J. Clim. 30, 1985–1997. https://doi.org/10.1175/JCLI-D-16-0396.1

Deser, C., Alexander, M.A., Xie, S.-P., Phillips, A.S., 2010. Sea Surface Temperature Variability: Patterns and Mechanisms. Annu. Rev. Mar. Sci. 2, 115–143. https://doi.org/10.1146/annurev-marine-120408-151453

Driscoll, S., Bozzo, A., Gray, L.J., Robock, A., Stenchikov, G., 2012. Coupled Model Intercomparison Project 5 (CMIP5) simulations of climate following volcanic eruptions. J. Geophys. Res. Atmospheres 117, n/a-n/a. https://doi.org/10.1029/2012JD017607

Duchez, A., Frajka-Williams, E., Josey, S.A., Evans, D.G., Grist, J.P., Marsh, R., McCarthy, G.D., Sinha, B., Berry, D.I., Hirschi, J.J.-M., 2016. Drivers of exceptionally cold North Atlantic Ocean temperatures and their link to the 2015 European heat wave. Environ. Res. Lett. 11, 074004. https://doi.org/10.1088/1748-9326/11/7/074004

Ebojie, F., Burrows, J.P., Gebhardt, C., Ladstätter-Weißenmayer, A., von Savigny, C., Rozanov, A., Weber, M., Bovensmann, H., 2016. Global tropospheric ozone variations from 2003 to 2011 as seen by SCIAMACHY. Atmospheric Chem. Phys. 16, 417–436. https://doi.org/10.5194/acp-16-417-2016

Eden, C., Willebrand, J., 2001. Mechanism of Interannual to Decadal Variability of the North Atlantic Circulation. J. Clim. 14, 2266–2280. https://doi.org/10.1175/1520-0442(2001)014<2266:MOITDV>2.0.CO;2

Enderlin, E.M., Howat, I.M., Jeong, S., Noh, M.-J., van Angelen, J.H., van den Broeke, M.R., 2014. An improved mass budget for the Greenland ice sheet. Geophys. Res. Lett. 41, 866–872. https://doi.org/10.1002/2013GL059010

Fereday, D.R., Maidens, A., Arribas, A., Scaife, A.A., Knight, J.R., 2012. Seasonal forecasts of northern hemisphere winter 2009/10. Environ. Res. Lett. 7, 034031. https://doi.org/10.1088/1748-9326/7/3/034031

Fettweis, X., Hanna, E., Lang, C., Belleflamme, A., Erpicum, M., Gallée, H., 2013. Brief communication: "Important role of the mid-tropospheric atmospheric circulation in the recent surface melt increase over the Greenland ice sheet." The Cryosphere 7, 241–248. https://doi.org/10.5194/tc-7-241-2013

Fettweis, X., Mabille, G., Erpicum, M., Nicolay, S., den Broeke, M.V., 2011. The 1958–2009 Greenland ice sheet surface melt and the mid-tropospheric atmospheric circulation. Clim. Dyn. 36, 139–159. https://doi.org/10.1007/s00382-010-0772-8

Foukal, N.P., Lozier, M.S., 2017. Assessing variability in the size and strength of the North Atlantic subpolar gyre: NORTH ATLANTIC SUBPOLAR GYRE VARIABILITY. J. Geophys. Res. Oceans 122, 6295–6308. https://doi.org/10.1002/2017JC012798

Frajka-Williams, E., Lankhorst, M., Koelling, J., Send, U., 2016. Coherent changes of the circulation in the deep North Atlantic from moored transport arrays. ArXiv161006708 Phys.

Gastineau, G., D'Andrea, F., Frankignoul, C., 2013. Atmospheric response to the North Atlantic Ocean variability on seasonal to decadal time scales. Clim. Dyn. 40, 2311–2330. https://doi.org/10.1007/s00382-012-1333-0

Gastineau, G., Frankignoul, C., 2014. Influence of the North Atlantic SST Variability on the Atmospheric Circulation during the Twentieth Century. J. Clim. 28, 1396–1416. https://doi.org/10.1175/JCLI-D-14-00424.1

Good, S.A., Martin, M.J., Rayner, N.A., 2013. EN4: Quality controlled ocean temperature and salinity profiles and monthly objective analyses with uncertainty estimates. J. Geophys. Res. Oceans 118, 6704–6716. https://doi.org/10.1002/2013JC009067

Granier, C., Bessagnet, B., Bond, T., D'Angiola, A., Denier van der Gon, H., Frost, G.J., Heil, A., Kaiser, J.W., Kinne, S., Klimont, Z., Kloster, S., Lamarque, J.-F., Liousse, C., Masui, T., Meleux, F., Mieville, A., Ohara, T., Raut, J.-C., Riahi, K., Schultz, M.G., Smith, S.J., Thompson, A., van Aardenne, J., van der Werf, G.R., van Vuuren, D.P., 2011. Evolution of anthropogenic and biomass burning emissions of air pollutants at global and regional scales during the 1980–2010 period. Clim. Change 109, 163–190. https://doi.org/10.1007/s10584-011-0154-1

Gray, L.J., Beer, J., Geller, M., Haigh, J.D., Lockwood, M., Matthes, K., Cubasch, U., Fleitmann, D., Harrison, G., Hood, L., others, 2010. Solar influences on climate. Rev. Geophys. 48.

Gray, L.J., Scaife, A.A., Mitchell, D.M., Osprey, S., Ineson, S., Hardiman, S., Butchart, N., Knight, J., Sutton, R., Kodera, K., 2013. A lagged response to the 11 year solar cycle in observed winter Atlantic/European weather patterns. J. Geophys. Res. Atmospheres 118.

Gray, L.J., Woollings, T.J., Andrews, M., Knight, J., 2016. Eleven-year solar cycle signal in the NAO and Atlantic/European blocking: 11-Year Solar Cycle in NAO and Atlantic/European Blocking. Q. J. R. Meteorol. Soc. 142, 1890–1903. https://doi.org/10.1002/qj.2782

Grist, J.P., Josey, S.A., Jacobs, Z.L., Marsh, R., Sinha, B., Van Sebille, E., 2016. Extreme air–sea interaction over the North Atlantic subpolar gyre during the winter of 2013–2014 and its sub-surface legacy. Clim. Dyn. 46, 4027–4045. https://doi.org/10.1007/s00382-015-2819-3

Häkkinen, S., Rhines, P.B., 2004. Decline of Subpolar North Atlantic Circulation During the 1990s. Science 304, 555–559. https://doi.org/10.1126/science.1094917

Hakkinen, S., Rhines, P.B., Worthen, D.L., 2011. Atmospheric Blocking and Atlantic Multidecadal Ocean Variability. Science 334, 655–659. https://doi.org/10.1126/science.1205683

Hanna, E., Fettweis, X., Mernild, S.H., Cappelen, J., Ribergaard, M.H., Shuman, C.A., Steffen, K., Wood, L., Mote, T.L., 2014. Atmospheric and oceanic climate forcing of the exceptional Greenland ice sheet surface melt in summer 2012. Int. J. Climatol. 34, 1022–1037. https://doi.org/10.1002/joc.3743

Hanna, E., Mernild, S.H., Cappelen, J., Steffen, K., 2012. Recent warming in Greenland in a long-term instrumental (1881–2012) climatic context: I. Evaluation of surface air temperature records. Environ. Res. Lett. 7, 045404. https://doi.org/10.1088/1748-9326/7/4/045404

Hansen, B., Húsgarð Larsen, K.M., Hátún, H., Østerhus, S., 2016. A stable Faroe Bank Channel overflow 1995–2015. Ocean Sci. 12, 1205–1220. https://doi.org/10.5194/os-12-1205-2016

Hartmann, D.L., Klein Tank, A.M., Rusticucci, M., Alexander, L.V., Brönnimann, S., Charabi, Y.A.R., Dentener, F.J., Dlugokencky, E.J., Easterling, D.R., Kaplan, A., others, 2013. Climate Change 2013 the Physical Science Basis: Working Group I Contribution to the Fifth Assessment Report of the Intergovernmental Panel on Climate Change, in: Cambridge University Press.

Hátún, H., Payne, M.R., Beaugrand, G., Reid, P.C., Sandø, A.B., Drange, H., Hansen, B., Jacobsen, J.A., Bloch, D., 2009. Large bio-geographical shifts in the north-eastern Atlantic Ocean: From the subpolar gyre, via plankton, to blue whiting and pilot whales. Prog. Oceanogr. 80, 149–162. https://doi.org/10.1016/j.pocean.2009.03.001

Hewitt, H.T., Copsey, D., Culverwell, I.D., Harris, C.M., Hill, R.S.R., Keen, A.B., McLaren, A.J., Hunke, E.C., 2011. Design and implementation of the infrastructure of HadGEM3: the next-generation Met Office climate modelling system. Geosci. Model Dev. 4, 223–253. https://doi.org/10.5194/gmd-4-223-2011

Hirschi, J., Marotzke, J., 2007. Reconstructing the Meridional Overturning Circulation from Boundary Densities and the Zonal Wind Stress. J. Phys. Oceanogr. 37, 743–763. https://doi.org/10.1175/JPO3019.1

Hoerling, M.P., Hurrell, J.W., Xu, T., Bates, G.T., Phillips, A.S., 2004. Twentieth century North Atlantic climate change. Part II: Understanding the effect of Indian Ocean warming. Clim. Dyn. 23. https://doi.org/10.1007/s00382-004-0433-x

Holland, D.M., Thomas, R.H., de Young, B., Ribergaard, M.H., Lyberth, B., 2008. Acceleration of Jakobshavn Isbræ triggered by warm subsurface ocean waters. Nat. Geosci. 1, 659–664. https://doi.org/10.1038/ngeo316

Hollmann, R., Merchant, C.J., Saunders, R., Downy, C., Buchwitz, M., Cazenave, A., Chuvieco, E., Defourny, P., de Leeuw, G., Forsberg, R., Holzer-Popp, T., Paul, F., Sandven, S., Sathyendranath, S., van Roozendael, M., Wagner, W., 2013. The ESA Climate Change Initiative: Satellite Data Records for Essential Climate Variables. Bull. Am. Meteorol. Soc. 94, 1541–1552. https://doi.org/10.1175/BAMS-D-11-00254.1

Huntingford, C., Marsh, T., Scaife, A.A., Kendon, E.J., Hannaford, J., Kay, A.L., Lockwood, M., Prudhomme, C., Reynard, N.S., Parry, S., Lowe, J.A., Screen, J.A., Ward, H.C., Roberts, M., Stott, P.A., Bell, V.A., Bailey, M., Jenkins, A., Legg, T., Otto, F.E.L., Massey, N., Schaller, N., Slingo, J., Allen, M.R., 2014. Potential influences on the United Kingdom's floods of winter 2013/14. Nat. Clim. Change 4, 769–777. https://doi.org/10.1038/nclimate2314

Hurrell, J.W., 1995. Decadal Trends in the North Atlantic Oscillation: Regional Temperatures and Precipitation. Science 269, 676–679. https://doi.org/10.1126/science.269.5224.676

Hurrell, J.W., Kushnir, Y., Ottersen, G., Visbeck, M., 2003. An overview of the North Atlantic Oscillation, in: Hurrell, J.W., Kushnir, Y., Ottersen, G., Visbeck, M. (Eds.), Geophysical Monograph Series. American Geophysical Union, Washington, D. C., pp. 1–35. https://doi.org/10.1029/134GM01

Ineson, S., Scaife, A.A., Knight, J.R., Manners, J.C., Dunstone, N.J., Gray, L.J., Haigh, J.D., 2011. Solar forcing of winter climate variability in the Northern Hemisphere. Nat. Geosci. 4, 753–757. https://doi.org/10.1038/ngeo1282

Jackson, L.C., Peterson, K.A., Roberts, C.D., Wood, R.A., 2016. Recent slowing of Atlantic overturning circulation as a recovery from earlier strengthening. Nat. Geosci. 9, 518–522. https://doi.org/10.1038/ngeo2715

Jochumsen, K., Quadfasel, D., Valdimarsson, H., Jónsson, S., 2012. Variability of the Denmark Strait overflow: Moored time series from 1996-2011: DENMARK STRAIT OVERFLOW. J. Geophys. Res. Oceans 117, n/a-n/a. https://doi.org/10.1029/2012JC008244

Jones, P.D., Jonsson, T., Wheeler, D., 1997. Extension to the North Atlantic oscillation using early instrumental pressure observations from Gibraltar and south-west Iceland. Int. J. Climatol. 17, 1433–1450. https://doi.org/10.1002/(SICI)1097-0088(19971115)17:13<1433::AID-JOC203>3.0.CO;2-P

Josey, S.A., Grist, J.P., Kieke, D., Yashayaev, I., Yu, L., 2015. Extraordinary Ocean Cooling and New Dense Water Formation in the North Atlantic, in "State of the Climate in 2014." Bull. Am. Meteorol. Soc. 96, S67–S68. https://doi.org/10.1175/2015BAMSStateoftheClimate

Joughin, I., Smith, B.E., Shean, D.E., Floricioiu, D., 2014. Brief Communication: Further summer speedup of Jakobshavn Isbræ. The Cryosphere 8, 209–214. https://doi.org/10.5194/tc-8-209-2014

Joyce, T.M., Zhang, R., 2010. On the Path of the Gulf Stream and the Atlantic Meridional Overturning Circulation. J. Clim. 23, 3146–3154. https://doi.org/10.1175/2010JCLI3310.1

Kampa, M., Castanas, E., 2008. Human health effects of air pollution. Environ. Pollut., Proceedings of the 4th International Workshop on Biomonitoring of Atmospheric Pollution (With Emphasis on Trace Elements) 151, 362–367. https://doi.org/10.1016/j.envpol.2007.06.012

Kanzow, T., Cunningham, S.A., Rayner, D., Hirschi, J.J.-M., Johns, W.E., Baringer, M.O., Bryden, H.L., Beal, L.M., Meinen, C.S., Marotzke, J., 2007. Observed Flow Compensation Associated with the MOC at 26.5 N in the Atlantic. Science 317, 938–941. https://doi.org/10.1126/science.1141293

Knight, J.R., 2005. A signature of persistent natural thermohaline circulation cycles in observed climate. Geophys. Res. Lett. 32. https://doi.org/10.1029/2005GL024233

Knight, J.R., Folland, C.K., Scaife, A.A., 2006. Climate impacts of the Atlantic Multidecadal Oscillation. Geophys. Res. Lett. 33. https://doi.org/10.1029/2006GL026242

Korhonen, H., Carslaw, K.S., Forster, P.M., Mikkonen, S., Gordon, N.D., Kokkola, H., 2010. Aerosol climate feedback due to decadal increases in Southern Hemisphere wind speeds: AEROSOL FEEDBACK DUE TO WIND SPEED. Geophys. Res. Lett. 37, n/a-n/a. https://doi.org/10.1029/2009GL041320

Kuipers Munneke, P., Ligtenberg, S.R.M., Noël, B.P.Y., Howat, I.M., Box, J.E., Mosley-Thompson, E., McConnell, J.R., Steffen, K., Harper, J.T., Das, S.B., van den Broeke, M.R., 2015. Elevation change of the Greenland Ice Sheet due to surface mass balance and firn processes, 1960–2014. The Cryosphere 9, 2009–2025. https://doi.org/10.5194/tc-9-2009-2015

Kwok, R., Cunningham, G.F., Wensnahan, M., Rigor, I., Zwally, H.J., Yi, D., 2009. Thinning and volume loss of the Arctic Ocean sea ice cover: 2003–2008. J. Geophys. Res. Oceans 114, C07005. https://doi.org/10.1029/2009JC005312

Landerer, F.W., Wiese, D.N., Bentel, K., Boening, C., Watkins, M.M., 2015. North Atlantic meridional overturning circulation variations from GRACE ocean bottom pressure anomalies. Geophys. Res. Lett. 42, 2015GL065730. https://doi.org/10.1002/2015GL065730

Lazier, J., Hendry, R., Clarke, A., Yashayaev, I., Rhines, P., 2002. Convection and restratification in the Labrador Sea, 1990 2000. Deep Sea Res. Part Oceanogr. Res. 49, 1819–1835. https://doi.org/10.1016/S0967-0637(02)00064-X

Lewis, R., Schwartz, E., 2004. Sea Salt Aerosol Production: Mechanisms, Methods, Measurements and Models—A Critical Review, Geophysical Monograph Series. American Geophysical Union, Washington, D. C. https://doi.org/10.1029/GM152

Li, Q., Jacob, D.J., Bey, I., Palmer, P.I., Duncan, B.N., Field, B.D., Martin, R.V., Fiore, A.M., Yantosca, R.M., Parrish, D.D., Simmonds, P.G., Oltmans, S.J., 2002. Transatlantic transport of pollution and its effects on surface ozone in Europe and North America. J. Geophys. Res. Atmospheres 107, ACH 4-1. https://doi.org/10.1029/2001JD001422

Lozier, M.S., Gary, S.F., Bower, A.S., 2013. Simulated pathways of the overflow waters in the North Atlantic: Subpolar to subtropical export. Deep Sea Res. Part II Top. Stud. Oceanogr. 85, 147–153. https://doi.org/10.1016/j.dsr2.2012.07.037

Maidens, A., Arribas, A., Scaife, A.A., MacLachlan, C., Peterson, D., Knight, J., 2013. The Influence of Surface Forcings on Prediction of the North Atlantic Oscillation Regime of Winter 2010/11. Mon. Weather Rev. 141, 3801–3813. https://doi.org/10.1175/MWR-D-13-00033.1

Malley, C.S., Henze, D.K., Kuylenstierna, J.C.I., Vallack, H.W., Davila, Y., Anenberg, S.C., Turner, M.C., Ashmore, M.R., 2017. Updated Global Estimates of Respiratory Mortality in Adults

≥30Years of Age Attributable to Long-Term Ozone Exposure. Environ. Health Perspect. 125. https://doi.org/10.1289/EHP1390
Marshall, A.G., Scaife, A.A., 2009. Impact of the QBO on surface winter climate. J. Geophys. Res. 114. https://doi.org/10.1029/2009JD011737
Mauritzen, C., Melsom, A., Sutton, R.T., 2012. Importance of density-compensated temperature change for deep North Atlantic Ocean heat uptake. Nat. Geosci. 5, 905–910. https://doi.org/10.1038/ngeo1639
McCarthy, G., Frajka-Williams, E., Johns, W.E., Baringer, M.O., Meinen, C.S., Bryden, H.L., Rayner, D., Duchez, A., Roberts, C., Cunningham, S.A., 2012. Observed interannual variability of the Atlantic meridional overturning circulation at 26.5°N. Geophys. Res. Lett. 39, n/a-n/a. https://doi.org/10.1029/2012GL052933
McCarthy, G.D., Haigh, I.D., Hirschi, J.J.-M., Grist, J.P., Smeed, D.A., 2015. Ocean impact on decadal Atlantic climate variability revealed by sea-level observations. Nature 521, 508–510. https://doi.org/10.1038/nature14491
McCarthy, G.D., Menary, M.B., Mecking, J.V., Moat, B.I., Johns, W.E., Andrews, M., Rayner, D., Smeed, D.A., 2017. The importance of deep, basinwide measurements in optimised Atlantic Meridional Overturning Circulation observing arrays. J. Geophys. Res. 1808–1826.
McCarthy, G.D., Smeed, D.A., Johns, W.E., Frajka-Williams, E., Moat, B.I., Rayner, D., Baringer, M.O., Meinen, C.S., Collins, J., Bryden, H.L., 2015. Measuring the Atlantic Meridional Overturning Circulation at 26°N. Prog. Oceanogr. 130, 91–111. https://doi.org/10.1016/j.pocean.2014.10.006
McMillan, M., Leeson, A., Shepherd, A., Briggs, K., Armitage, T.W.K., Hogg, A., Kuipers Munneke, P., van den Broeke, M., Noël, B., van de Berg, W.J., Ligtenberg, S., Horwath, M., Groh, A., Muir, A., Gilbert, L., 2016. A high-resolution record of Greenland mass balance: High-Resolution Greenland Mass Balance. Geophys. Res. Lett. 43, 7002–7010. https://doi.org/10.1002/2016GL069666
Menary, M.B., Hodson, D.L.R., Robson, J.I., Sutton, R.T., Wood, R.A., 2015. A Mechanism of Internal Decadal Atlantic Ocean Variability in a High-Resolution Coupled Climate Model. J. Clim. 28, 7764–7785. https://doi.org/10.1175/JCLI-D-15-0106.1
Menary, M.B., Roberts, C.D., Palmer, M.D., Halloran, P.R., Jackson, L., Wood, R.A., Mueller, W.A., Matei, D., Lee, S.-K., 2013. Mechanisms of aerosol-forced AMOC variability in a state of the art climate model. J. Geophys. Res. Oceans 118, 2087–2096.
Merchant, C.J., Embury, O., Roberts-Jones, J., Fiedler, E., Bulgin, C.E., Corlett, G.K., Good, S., McLaren, A., Rayner, N., Morak-Bozzo, S., Donlon, C., 2014. Sea surface temperature datasets for climate applications from Phase 1 of the European Space Agency Climate Change Initiative (SST CCI). Geosci. Data J. 1, 179–191. https://doi.org/10.1002/gdj3.20
Mickley, L.J., Jacob, D.J., Rind, D., 2001. Uncertainty in preindustrial abundance of tropospheric ozone: Implications for radiative forcing calculations. J. Geophys. Res. Atmospheres 106, 3389–3399. https://doi.org/10.1029/2000JD900594
Monks, P.S., Archibald, A.T., Colette, A., Cooper, O., Coyle, M., Derwent, R., Fowler, D., Granier, C., Law, K.S., Mills, G.E., Stevenson, D.S., Tarasova, O., Thouret, V., von Schneidemesser, E., Sommariva, R., Wild, O., Williams, M.L., 2015. Tropospheric ozone and its precursors from the urban to the global scale from air quality to short-lived climate forcer. Atmos Chem Phys 15, 8889–8973. https://doi.org/10.5194/acp-15-8889-2015

Neu, J.L., Flury, T., Manney, G.L., Santee, M.L., Livesey, N.J., Worden, J., 2014. Tropospheric ozone variations governed by changes in stratospheric circulation. Nat. Geosci. 7, 340–344. https://doi.org/10.1038/ngeo2138

Nghiem, S.V., Hall, D.K., Mote, T.L., Tedesco, M., Albert, M.R., Keegan, K., Shuman, C.A., DiGirolamo, N.E., Neumann, G., 2012. The extreme melt across the Greenland ice sheet in 2012. Geophys. Res. Lett. 39. https://doi.org/10.1029/2012GL053611

Nisbet, E.G., Dlugokencky, E.J., Manning, M.R., Lowry, D., Fisher, R.E., France, J.L., Michel, S.E., Miller, J.B., White, J.W.C., Vaughn, B., Bousquet, P., Pyle, J.A., Warwick, N.J., Cain, M., Brownlow, R., Zazzeri, G., Lanoisellé, M., Manning, A.C., Gloor, E., Worthy, D.E.J., Brunke, E.-G., Labuschagne, C., Wolff, E.W., Ganesan, A.L., 2016. Rising atmospheric methane: 2007–2014 growth and isotopic shift. Glob. Biogeochem. Cycles 30, 2016GB005406. https://doi.org/10.1002/2016GB005406

Oetjen, H., Payne, V.H., Neu, J.L., Kulawik, S.S., Edwards, D.P., Eldering, A., Worden, H.M., Worden, J.R., 2016. A joint data record of tropospheric ozone from Aura-TES and MetOp-IASI. Atmos Chem Phys 16, 10229–10239. https://doi.org/10.5194/acp-16-10229-2016

Omrani, N.-E., Bader, J., Keenlyside, N.S., Manzini, E., 2016. Troposphere–stratosphere response to large-scale North Atlantic Ocean variability in an atmosphere/ocean coupled model. Clim. Dyn. 46, 1397–1415. https://doi.org/10.1007/s00382-015-2654-6

O'Reilly, C.H., Minobe, S., Kuwano-Yoshida, A., Woollings, T., 2017. The Gulf Stream influence on wintertime North Atlantic jet variability. Q. J. R. Meteorol. Soc. 143, 173–183. https://doi.org/10.1002/qj.2907

Ortega, P., Hawkins, E., Sutton, R., 2011. Processes governing the predictability of the Atlantic meridional overturning circulation in a coupled GCM. Clim. Dyn. 37, 1771–1782. https://doi.org/10.1007/s00382-011-1025-1

Ortega, P., Lehner, F., Swingedouw, D., Masson-Delmotte, V., Raible, C.C., Casado, M., Yiou, P., 2015. A model-tested North Atlantic Oscillation reconstruction for the past millennium. Nature 523, 71–74. https://doi.org/10.1038/nature14518

Parrish, D.D., Lamarque, J.-F., Naik, V., Horowitz, L., Shindell, D.T., Staehelin, J., Derwent, R., Cooper, O.R., Tanimoto, H., Volz-Thomas, A., Gilge, S., Scheel, H.-E., Steinbacher, M., Fröhlich, M., 2014. Long-term changes in lower tropospheric baseline ozone concentrations: Comparing chemistry-climate models and observations at northern midlatitudes. J. Geophys. Res. Atmospheres 119, 5719–5736. https://doi.org/10.1002/2013JD021435

Pascoe, C.L., Gray, L.J., Scaife, A.A., 2006. A GCM study of the influence of equatorial winds on the timing of sudden stratospheric warmings. Geophys. Res. Lett. 33. https://doi.org/10.1029/2005GL024715

Pausata, F.S.R., Pozzoli, L., Vignati, E., Dentener, F.J., 2012. North Atlantic Oscillation and tropospheric ozone variability in Europe: model analysis and measurements intercomparison. Atmospheric Chem. Phys. 12, 6357–6376. https://doi.org/10.5194/acp-12-6357-2012

Peings, Y., Magnusdottir, G., 2014. Forcing of the wintertime atmospheric circulation by the multidecadal fluctuations of the North Atlantic ocean. Environ. Res. Lett. 9, 034018. https://doi.org/10.1088/1748-9326/9/3/034018

Poulsen, C.A., Watts, P.D., Thomas, G.E., Sayer, A.M., Siddans, R., Grainger, R.G., Lawrence, B.N., Campmany, E., Dean, S.M., Arnold, C., 2011. Cloud retrievals from satellite data using

optimal estimation: evaluation and application to ATSR. Atmospheric Meas. Tech. Discuss. 4, 2389–2431. https://doi.org/10.5194/amtd-4-2389-2011
Prather, M.J., Holmes, C.D., 2017. Overexplaining or underexplaining methane's role in climate change. Proc. Natl. Acad. Sci. 114, 5324–5326. https://doi.org/10.1073/pnas.1704884114
Read, K.A., Mahajan, A.S., Carpenter, L.J., Evans, M.J., Faria, B.V.E., Heard, D.E., Hopkins, J.R., Lee, J.D., Moller, S.J., Lewis, A.C., Mendes, L., McQuaid, J.B., Oetjen, H., Saiz-Lopez, A., Pilling, M.J., Plane, J.M.C., 2008. Extensive halogen-mediated ozone destruction over the tropical Atlantic Ocean. Nature 453, 1232–1235. https://doi.org/10.1038/nature07035
Rigby, M., Montzka, S.A., Prinn, R.G., White, J.W.C., Young, D., O?Doherty, S., Lunt, M.F., Ganesan, A.L., Manning, A.J., Simmonds, P.G., Salameh, P.K., Harth, C.M., M?hle, J., Weiss, R.F., Fraser, P.J., Steele, L.P., Krummel, P.B., McCulloch, A., Park, S., 2017. Role of atmospheric oxidation in recent methane growth. Proc. Natl. Acad. Sci. 114, 5373–5377. https://doi.org/10.1073/pnas.1616426114
Rignot, E., Koppes, M., Velicogna, I., 2010. Rapid submarine melting of the calving faces of West Greenland glaciers. Nat. Geosci. 3, 187–191. https://doi.org/10.1038/ngeo765
Rignot, E., Velicogna, I., van den Broeke, M.R., Monaghan, A., Lenaerts, J.T.M., 2011. Acceleration of the contribution of the Greenland and Antarctic ice sheets to sea level rise: ACCELERATION OF ICE SHEET LOSS. Geophys. Res. Lett. 38, n/a-n/a. https://doi.org/10.1029/2011GL046583
Roberts, C.D., Waters, J., Peterson, K.A., Palmer, M.D., McCarthy, G.D., Frajka-Williams, E., Haines, K., Lea, D.J., Martin, M.J., Storkey, D., Blockley, E.W., Zuo, H., 2013. Atmosphere drives recent interannual variability of the Atlantic meridional overturning circulation at 26.5°N. Geophys. Res. Lett. 40, 5164–5170. https://doi.org/10.1002/grl.50930
Roberts, J.F., Champion, A.J., Dawkins, L.C., Hodges, K.I., Shaffrey, L.C., Stephenson, D.B., Stringer, M.A., Thornton, H.E., Youngman, B.D., 2014. The XWS open access catalogue of extreme European windstorms from 1979 to 2012. Nat Hazards Earth Syst Sci 14, 2487–2501. https://doi.org/10.5194/nhess-14-2487-2014
Robson, J., Hodson, D., Hawkins, E., Sutton, R., 2014. Atlantic overturning in decline? Nat. Geosci. 7, 2–3. https://doi.org/10.1038/ngeo2050
Robson, J., Ortega, P., Sutton, R., 2016. A reversal of climatic trends in the North Atlantic since 2005. Nat. Geosci. 9, 513–517. https://doi.org/10.1038/ngeo2727
Robson, J., Sutton, R., Lohmann, K., Smith, D., Palmer, M.D., 2012. Causes of the Rapid Warming of the North Atlantic Ocean in the Mid-1990s. J. Clim. 25, 4116–4134. https://doi.org/10.1175/JCLI-D-11-00443.1
Scaife, A.A., Comer, R., Dunstone, N., Fereday, D., Folland, C., Good, E., Gordon, M., Hermanson, L., Ineson, S., Karpechko, A., Knight, J., MacLachlan, C., Maidens, A., Peterson, K.A., Smith, D., Slingo, J., Walker, B., 2017. Predictability of European winter 2015/2016. Atmospheric Sci. Lett. 18, 38–44. https://doi.org/10.1002/asl.721
Scaife, A.A., Folland, C.K., Alexander, L.V., Moberg, A., Knight, J.R., 2008. European Climate Extremes and the North Atlantic Oscillation. J. Clim. 21, 72–83. https://doi.org/10.1175/2007JCLI1631.1
Scaife, A.A., Knight, J.R., Vallis, G.K., Folland, C.K., 2005. A stratospheric influence on the winter NAO and North Atlantic surface climate. Geophys. Res. Lett. 32, L18715. https://doi.org/10.1029/2005GL023226
Schaefer, H., Fletcher, S.E.M., Veidt, C., Lassey, K.R., Brailsford, G.W., Bromley, T.M., Dlugokencky, E.J., Michel, S.E., Miller, J.B., Levin, I., Lowe, D.C., Martin, R.J., Vaughn, B.H., White, J.W.C.,

2016. A 21st century shift from fossil-fuel to biogenic methane emissions indicated by 13CH4. Science aad2705. https://doi.org/10.1126/science.aad2705
Seager, R., Kushnir, Y., Nakamura, J., Ting, M., Naik, N., 2010. Northern Hemisphere winter snow anomalies: ENSO, NAO and the winter of 2009/10. Geophys. Res. Lett. 37, L14703. https://doi.org/10.1029/2010GL043830
Semenov, V.A., Latif, M., Jungclaus, J.H., Park, W., 2008. Is the observed NAO variability during the instrumental record unusual? Geophys. Res. Lett. 35. https://doi.org/10.1029/2008GL033273
Shepherd, A., Ivins, E.R., A, G., Barletta, V.R., Bentley, M.J., Bettadpur, S., Briggs, K.H., Bromwich, D.H., Forsberg, R., Galin, N., Horwath, M., Jacobs, S., Joughin, I., King, M.A., Lenaerts, J.T.M., Li, J., Ligtenberg, S.R.M., Luckman, A., Luthcke, S.B., McMillan, M., Meister, R., Milne, G., Mouginot, J., Muir, A., Nicolas, J.P., Paden, J., Payne, A.J., Pritchard, H., Rignot, E., Rott, H., Sorensen, L.S., Scambos, T.A., Scheuchl, B., Schrama, E.J.O., Smith, B., Sundal, A.V., van Angelen, J.H., van de Berg, W.J., van den Broeke, M.R., Vaughan, D.G., Velicogna, I., Wahr, J., Whitehouse, P.L., Wingham, D.J., Yi, D., Young, D., Zwally, H.J., 2012. A Reconciled Estimate of Ice-Sheet Mass Balance. Science 338, 1183–1189. https://doi.org/10.1126/science.1228102
Shindell, D., Faluvegi, G., Lacis, A., Hansen, J., Ruedy, R., Aguilar, E., 2006. Role of tropospheric ozone increases in 20th-century climate change. J. Geophys. Res. 111. https://doi.org/10.1029/2005JD006348
Simmonds, P.G., Manning, A.J., Athanassiadou, M., Scaife, A.A., Derwent, R.G., O'Doherty, S., Harth, C.M., Weiss, R.F., Dutton, G.S., Hall, B.D., Sweeney, C., Elkins, J.W., 2013. Interannual fluctuations in the seasonal cycle of nitrous oxide and chlorofluorocarbons due to the Brewer-Dobson circulation: SEASONAL AMPLITUDE OF N_2O AND CFCs. J. Geophys. Res. Atmospheres 118, 10,694-10,706. https://doi.org/10.1002/jgrd.50832
Smeed, D.A., McCarthy, G.D., Cunningham, S.A., Frajka-Williams, E., Rayner, D., Johns, W.E., Meinen, C.S., Baringer, M.O., Moat, B.I., Duchez, A., Bryden, H.L., 2014. Observed decline of the Atlantic meridional overturning circulation 2004-2012. Ocean Sci. 10, 29–38. https://doi.org/10.5194/os-10-29-2014
Smith, D.M., Eade, R., Dunstone, N.J., Fereday, D., Murphy, J.M., Pohlmann, H., Scaife, A.A., 2010. Skilful multi-year predictions of Atlantic hurricane frequency. Nat. Geosci. 3, 846–849. https://doi.org/10.1038/ngeo1004
Stephens, G.L., Gabriel, P.M., Partain, P.T., 2001. Parameterization of Atmospheric Radiative Transfer. Part I: Validity of Simple Models. J. Atmospheric Sci. 58, 3391–3409. https://doi.org/10.1175/1520-0469(2001)058<3391:POARTP>2.0.CO;2
Stevenson, D.S., Young, P.J., Naik, V., Lamarque, J.-F., Shindell, D.T., Voulgarakis, A., Skeie, R.B., Dalsoren, S.B., Myhre, G., Berntsen, T.K., Folberth, G.A., Rumbold, S.T., Collins, W.J., MacKenzie, I.A., Doherty, R.M., Zeng, G., van Noije, T.P.C., Strunk, A., Bergmann, D., Cameron-Smith, P., Plummer, D.A., Strode, S.A., Horowitz, L., Lee, Y.H., Szopa, S., Sudo, K., Nagashima, T., Josse, B., Cionni, I., Righi, M., Eyring, V., Conley, A., Bowman, K.W., Wild, O., Archibald, A., 2013. Tropospheric ozone changes, radiative forcing and attribution to emissions in the Atmospheric Chemistry and Climate Model Intercomparison Project (ACCMIP). Atmospheric Chem. Phys. 13, 3063–3085. https://doi.org/10.5194/acp-13-3063-2013
Stocker, T.F., Qin, D., Plattner, G.-K., Tignor, M., Allen, S.K., Boschung, J., Nauels, A., Xia, Y., Bex, V., Midgley, P.M., others, 2013. Climate change 2013: The physical science basis. Intergov.

Panel Clim. Change Work. Group Contrib. IPCC Fifth Assess. Rep. AR5Cambridge Univ Press N. Y.
Sutton, R.T., Dong, B., 2012. Atlantic Ocean influence on a shift in European climate in the 1990s. Nat. Geosci. 5, 788–792. https://doi.org/10.1038/ngeo1595
Sutton, R.T., Hodson, D.L.R., 2005. Atlantic Ocean Forcing of North American and European Summer Climate. Science 309, 115–118. https://doi.org/10.1126/science.1109496
Sutton, R.T., McCarthy, G.D., Robson, J., Sinha, B., Archibald, A., Gray, L.J., 2017. Atlantic Multi-decadal Variability and the UK ACSIS programme. Bull. Am. Meteorol. Soc. https://doi.org/10.1175/BAMS-D-16-0266.1
Thomas, R., Frederick, E., Krabill, W., Manizade, S., Martin, C., 2006. Progressive increase in ice loss from Greenland: INCREASE IN ICE LOSS FROM GREENLAND. Geophys. Res. Lett. 33, n/a-n/a. https://doi.org/10.1029/2006GL026075
Tian, baijun, National Center for Atmospheric Research Staff (eds), 2016. The Climate Data Guide: AIRS and AMSU: Tropospheric air temperature and specific humidity. [WWW Document]. URL https://climatedataguide.ucar.edu/climate-data/airs-and-amsu-tropospheric-air-temperature-and-specific-humidity.
Tilling, R.L., Ridout, A., Shepherd, A., Wingham, D.J., 2015. Increased Arctic sea ice volume after anomalously low melting in 2013. Nat. Geosci. 8, 643–646. https://doi.org/10.1038/ngeo2489
Turner, A.J., Frankenberg, C., Wennberg, P.O., Jacob, D.J., 2017. Ambiguity in the causes for decadal trends in atmospheric methane and hydroxyl. Proc. Natl. Acad. Sci. 114, 5367–5372. https://doi.org/10.1073/pnas.1616020114
Twomey, S., 1974. Pollution and the planetary albedo. Atmospheric Environ. 1967 8, 1251–1256. https://doi.org/10.1016/0004-6981(74)90004-3
van den Broeke, M., Bamber, J., Ettema, J., Rignot, E., Schrama, E., van de Berg, W.J., van Meijgaard, E., Velicogna, I., Wouters, B., 2009. Partitioning Recent Greenland Mass Loss. Science 326, 984–986. https://doi.org/10.1126/science.1178176
Vaughan, D.G., Comiso, J.C., Allison, I., Carrasco, J., Kaser, G., Kwok, R., Mote, P., Murray, T., Paul, F., Ren, J., Rignot, E., 2013. Observations: Cryosphere., in: Climate Change 2013: Physical Science Basis. Contribution of Working Group I to the Fifth Assessment Report of the Intergovernmental Panel on Climate Change. Cambridge University Press, Cambridge, UK.
Watson, P.A.G., Weisheimer, A., Knight, J.R., Palmer, T.N., 2016. The role of the tropical West Pacific in the extreme Northern Hemisphere winter of 2013/2014. J. Geophys. Res. Atmospheres 121, 1698–1714. https://doi.org/10.1002/2015JD024048
Welti, A., Müller, K., Fleming, Z.L., Stratmann, F., 2017. Concentration and variability of ice nuclei in the subtropic, maritime boundary layer. Atmospheric Chem. Phys. Discuss. 1–18. https://doi.org/10.5194/acp-2017-783
Wigley, T.M.L., Santer, B.D., Lanzante, J.R., 2006. Appendix A: Statistical issues regarding trends., in: Karl, T.R., Hassol, S.J., Miller, C.D., Murray, W.L. (Eds.), Temperature Trends in the Lower Atmosphere: Steps for Understanding and Reconciling Differences. A Report by the U.S. Climate Change Science Program and the Subcommittee on Global Change Research, Washington DC.
Wild, S., Befort, D.J., Leckebusch, G.C., 2015. Was the Extreme Storm Season in Winter 2013/14 Over the North Atlantic and the United Kingdom Triggered by Changes in the West Pacific Warm Pool? Bull. Am. Meteorol. Soc. 96, S29–S34. https://doi.org/10.1175/BAMS-D-15-00118.1

Williams, R.G., Roussenov, V., Smith, D., Lozier, M.S., 2014. Decadal Evolution of Ocean Thermal Anomalies in the North Atlantic: The Effects of Ekman, Overturning, and Horizontal Transport. J. Clim. 27, 698–719. https://doi.org/10.1175/JCLI-D-12-00234.1

Wingham, D.J., Francis, C.R., Baker, S., Bouzinac, C., Brockley, D., Cullen, R., de Chateau-Thierry, P., Laxon, S.W., Mallow, U., Mavrocordatos, C., Phalippou, L., Ratier, G., Rey, L., Rostan, F., Viau, P., Wallis, D.W., 2006. CryoSat: A mission to determine the fluctuations in Earth's land and marine ice fields. Adv. Space Res., Natural Hazards and Oceanographic Processes from Satellite Data 37, 841–871. https://doi.org/10.1016/j.asr.2005.07.027

Woollings, T., Czuchnicki, C., Franzke, C., 2014. Twentieth century North Atlantic jet variability: Jet variability. Q. J. R. Meteorol. Soc. 140, 783–791. https://doi.org/10.1002/qj.2197

Woollings, T., Franzke, C., Hodson, D.L.R., Dong, B., Barnes, E.A., Raible, C.C., Pinto, J.G., 2015. Contrasting interannual and multidecadal NAO variability. Clim. Dyn. 45, 539–556.

Woollings, T., Gregory, J.M., Pinto, J.G., Reyers, M., Brayshaw, D.J., 2012. Response of the North Atlantic storm track to climate change shaped by ocean-atmosphere coupling. Nat. Geosci. 5, 313–317.

Worden, H.M., Deeter, M.N., Frankenberg, C., George, M., Nichitiu, F., Worden, J., Aben, I., Bowman, K.W., Clerbaux, C., Coheur, P.F., de Laat, A.T.J., Detweiler, R., Drummond, J.R., Edwards, D.P., Gille, J.C., Hurtmans, D., Luo, M., Martínez-Alonso, S., Massie, S., Pfister, G., Warner, J.X., 2013. Decadal record of satellite carbon monoxide observations. Atmospheric Chem. Phys. 13, 837–850. https://doi.org/10.5194/acp-13-837-2013

Xiong, X., Barnet, C., Maddy, E., Sweeney, C., Liu, X., Zhou, L., Goldberg, M., 2008. Characterization and validation of methane products from the Atmospheric Infrared Sounder (AIRS). J. Geophys. Res. 113. https://doi.org/10.1029/2007JG000500

Yashayaev, I., Loder, J.W., 2016. Recurrent replenishment of Labrador Sea Water and associated decadal-scale variability: 2015 Convection in Labrador Sea. J. Geophys. Res. Oceans 121, 8095–8114. https://doi.org/10.1002/2016JC012046

Yashayaev, I., van Aken, H.M., Holliday, N.P., Bersch, M., 2007. Transformation of the Labrador Sea Water in the subpolar North Atlantic. Geophys. Res. Lett. 34. https://doi.org/10.1029/2007GL031812

Young, P.J., Archibald, A.T., Bowman, K.W., Lamarque, J.-F., Naik, V., Stevenson, D.S., Tilmes, S., Voulgarakis, A., Wild, O., Bergmann, D., Cameron-Smith, P., Cionni, I., Collins, W.J., Dalsøren, S.B., Doherty, R.M., Eyring, V., Faluvegi, G., Horowitz, L.W., Josse, B., Lee, Y.H., MacKenzie, I.A., Nagashima, T., Plummer, D.A., Righi, M., Rumbold, S.T., Skeie, R.B., Shindell, D.T., Strode, S.A., Sudo, K., Szopa, S., Zeng, G., 2013. Pre-industrial to end 21st century projections of tropospheric ozone from the Atmospheric Chemistry and Climate Model Intercomparison Project (ACCMIP). Atmos Chem Phys 13, 2063–2090. https://doi.org/10.5194/acp-13-2063-2013

Yuan, T., Oreopoulos, L., Zelinka, M., Yu, H., Norris, J.R., Chin, M., Platnick, S., Meyer, K., 2016. Positive low cloud and dust feedbacks amplify tropical North Atlantic Multidecadal Oscillation. Geophys. Res. Lett. 43, 1349–1356. https://doi.org/10.1002/2016GL067679

Yurganov, L.N., McMillan, W.W., Dzhola, A.V., Grechko, E.I., Jones, N.B., van der Werf, G.R., 2008. Global AIRS and MOPITT CO measurements: Validation, comparison, and links to biomass burning variations and carbon cycle. J. Geophys. Res. 113. https://doi.org/10.1029/2007JD009229

Zhang, R., Delworth, T.L., 2006. Impact of Atlantic multidecadal oscillations on India/Sahel rainfall and Atlantic hurricanes. Geophys. Res. Lett. 33.

1434 Ziemke, J.R., Chandra, S., Duncan, B.N., Froidevaux, L., Bhartia, P.K., Levelt, P.F., Waters, J.W.,
1435 2006. Tropospheric ozone determined from Aura OMI and MLS: Evaluation of
1436 measurements and comparison with the Global Modeling Initiative's Chemical Transport
1437 Model. J. Geophys. Res. 111. https://doi.org/10.1029/2006JD007089
1438